Available online at www.sciencedirect.com
ScienceDirect
Geochimica et Cosmochimica Acta 71 (2007) 2326–2343
Geochimica et Cosmochimica Acta
www.elsevier.com/locate/gca

Rare sulfur and triple oxygen isotope geochemistry of volcanogenic sulfate aerosols

I.N. Bindeman [a,*], J.M. Eiler [b], B.A. Wing [c,d], J. Farquhar [d,e]

[a] Department of Geological Sciences, University of Oregon, Eugene, OR 97403-1272, USA
[b] Geological and Planetary Sciences, California Institute of Technology, Pasadena, CA, USA
[c] Department of Earth and Planetary Sciences, McGill University, Montreal, Que., Canada
[d] Department of Geology and Earth System Science Interdisciplinary Center, University of Maryland, College Park, MD, USA
[e] Hanse-Wissenschaftskolleg (HWK), Lehmkuhlenbusch 4, 27753 Delmenhorst, Germany

Received 25 April 2006; accepted in revised form 29 January 2007; available online 8 February 2007

Abstract

We present analyses of stable isotopic ratios $^{17}O/^{16}O$, $^{18}O/^{16}O$, $^{34}S/^{32}S$, and $^{33}S/^{32}S$, $^{36}S/^{32}S$ in sulfate leached from volcanic ash of a series of well known, large and small volcanic eruptions. We consider eruptions of Mt. St. Helens (Washington, 1980, ~1 km^3), Mt. Spurr (Alaska, 1953, <1 km^3), Gjalp (Iceland, 1996, 1998, <1 km^3), Pinatubo (Phillipines, 1991, 10 km^3), Bishop tuff (Long Valley, California, 0.76 Ma, 750 km^3), Lower Bandelier tuff (Toledo Caldera, New Mexico, 1.61 Ma, 600 km^3), and Lava Creek and Huckleberry Ridge tuffs (Yellowstone, Wyoming, 0.64 Ma, 1000 km^3 and 2.04 Ma 2500 km^3, respectively). This list covers much of the diversity of sizes and the character of silicic volcanic eruptions. Particular emphasis is paid to the Lava Creek tuff for which we present wide geographic sample coverage.

This global dataset spans a significant range in $\delta^{34}S$, $\delta^{18}O$, and $\Delta^{17}O$ of sulfate (29‰, 30‰, and 3.3‰, respectively) with oxygen isotopes recording mass-independent ($\Delta^{17}O > 0.2$‰) and sulfur isotopes exhibiting mass-dependent behavior. Products of large eruptions account for most of these isotopic ranges. Sulfate with $\Delta^{17}O > 0.2$‰ is present as 1–10 μm gypsum crystals on distal ash particles and records the isotopic signature of stratospheric photochemical reactions. Sediments that embed ash layers do not contain sulfate or contain little sulfate with $\Delta^{17}O$ near 0‰, suggesting that the observed sulfate in ash is of volcanic origin.

Mass-dependent fractionation of sulfur isotopic ratios suggests that sulfate-forming reactions did not involve photolysis of SO_2, like that inferred for pre-2.3 Ga sulfates from Archean sediments or Antarctic ice-core sulfate associated with few dated eruptions. Even though the sulfate sulfur isotopic compositions reflect mass-dependent processes, the products of caldera-forming eruptions display a large $\delta^{34}S$ range and exhibit fractionation relationships that do not follow the expected equilibrium slopes of 0.515 and 1.90 for $^{33}S/^{32}S$ vs. $^{34}S/^{32}S$ and $^{36}S/^{32}S$ vs. $^{34}S/^{32}S$, respectively. The data presented here are consistent with modification of a chemical mass-dependent fractionation of sulfur isotopes in the volcanic plume by either a kinetic gas phase reaction of volcanic SO_2 with OH and/or a Rayleigh processes involving a residual Rayleigh reactant—volcanic SO_2 gas, rather than a Rayleigh product. These results may also imply at least two removal pathways for SO_2 in volcanic plumes.

Above-zero $\Delta^{17}O$ values and their positive correlation with $\delta^{18}O$ in sulfate can be explained by oxidation by high-$\delta^{18}O$ and high-$\Delta^{17}O$ compounds such as ozone and radicals such as OH that result from ozone break down. Large caldera-forming eruptions have the highest $\Delta^{17}O$ values, and the largest range of $\delta^{18}O$, which can be explained by stratospheric reaction with ozone-derived OH radicals. These results suggest that massive eruptions are capable of causing a temporary depletion of the ozone layer. Such depletion may be many times that of the measured 3–8% depletion following 1991 Pinatubo eruption, if the amount of sulfur dioxide released scales with the amount of ozone depletion.

* Corresponding author.
E-mail address: bindeman@uoregon.edu (I.N. Bindeman).

0016-7037/$ - see front matter © 2007 Elsevier Ltd. All rights reserved.
doi:10.1016/j.gca.2007.01.026

1. INTRODUCTION

1.1. Volcanic aerosols and climate models

The long- and short-term influence of volcanic eruptions on global climate and atmospheric chemistry is a subject of much recent study (Coffey, 1996; Robock, 2000, 2002). Sulfur dioxide is the main volcanic compound that causes climatic cooling, primarily through oxidation to sulfuric acid aerosols; the aerosols scatter light in the stratosphere leading to stratospheric heating and surface cooling (Finlayson-Pitts and Pitts, 2000). The release of massive quantities of sulfur dioxide after large eruptions produces a significant impact on the environment and human evolution (e.g., Rampino and Self, 1992; Ambrose, 1998; Thordarson and Self, 2003; Bindeman, 2006). Rampino and Self (1992) and Ambrose (1998) hypothesized that the 74 ka Toba eruption in Indonesia had caused mass extinction and a "bottleneck" of early human evolution. Others interpret the coincidence to be casual and climatic impact of this eruption to be much more subdued (Oppenheimer, 2002).

Numerical models of climate forcing due to "sudden contaminant release" including sulfate aerosols are being developed (e.g., Bekki et al., 1996). However, modeling of the influence of large-scale volcanic eruptions on the atmosphere and climate presents significant challenges due to multiple physical and chemical feedbacks (Robock, 2000). Although many of these feedbacks include sulfate aerosol as a main player, the duration of climate cooling events after large eruptions are difficult to extrapolate numerically based on the effects of smaller eruptions (Robock, 2000, 2002). The 1–5 Gt sulfur dioxide release after the Toba eruption calls for dry fogs lasting for 6 years, as evidenced by the thickness of the H_2SO_4 layer in annual Antarctic ice-core records (Zielinski et al., 1996). Estimates of stratospheric sulfate loading after ejection of shallow marine and evaporitic deposits following 65 a Chicxulub impact event range from 30 to 300 Gt (Pierazzo et al., 2003); model calculations by these authors call for 2–8 °C global cooling of the surface for 5–6 years. This compares to <1 °C cooling after a much smaller eruption of Laki in Iceland or the 1815 eruption of Tambora (Indonesia), each of which released ~200–250 Mt of SO_2 gas (Thordarson and Self, 2003).

In addition to the complex climatic effects of volcanic sulfate aerosols, the amount of volcanic sulfate that actually makes it into the stratosphere remains largely unconstrained. The amount of SO_2 released to the upper troposphere and stratosphere per cubic kilometer of erupted material may vary by two orders of magnitude. A so-called sulfur excess paradox (e.g., Pyle et al., 1996; Wallace, 2003) calls for the presence of SO_2-rich gas bubbles in many magma chambers prior to eruption. However, most volcanic S-bearing gases are scavenged in the rising plume through reaction with volcanic and tropospherically derived water and OH radicals (Coffey, 1996) causing rapid oxidation and fallout of H_2SO_4 droplets in the vicinity of eruptive centers (Textor et al., 2003). In summary, the quantities of sulfur dioxide that reach the stratosphere, and the atmospheric response to the introduction of gigaton quantities of injected sulfur aerosols by large eruptions and meteorite impacts, are significant and at present can only be extrapolated with theoretical models and using evidence from smaller eruptions (e.g., Pierazzo et al., 2003).

1.2. O and S isotopes in sulfate from volcanic eruptions

Investigation of mass-dependent and mass-independent isotope effects of oxygen and sulfur (Thiemens, 2002) during release, transport, and oxidation of volcanically produced sulfur dioxide may provide an important independent tool to study physical and chemical changes of the atmosphere after volcanic eruptions. In particular, this approach may be relevant to understanding the magnitude of ozone and OH depletions following past eruptions. For example, the recent study by Savarino et al. (2003a) focused on sulfate peaks in Antarctic ice cores that correspond to large-volume volcanic events of the last ~1000 years. Surprisingly they found much smaller $\Delta^{17}O$ anomalies in the sulfate from the ~1200 AD acidic peak associated with the unknown large-volume volcanic event of the 13th century than in the sulfate associated with the 1991 AD Plinian eruption of Pinatubo, despite significantly higher H_2SO_4 concentrations—and presumably a much larger volume eruption—associated with the unknown event. On the basis of their isotopic measurements, Savarino et al. (2003a) concluded that larger eruptive events may leave a record of near zero $\Delta^{17}O$ values in ice cores. Exploratory photochemical modeling indicated that large volumes of SO_2 gas associated with super eruptions may "dry out" the stratosphere by essentially tritrating out OH (Savarino et al., 2003a). In turn, this would result in a change of the SO_2 oxidation pathway, which then proceeds via reaction with $O(^3P)$ (Bekki, 1995; Lyons, 2001; Savarino et al., 2003a). Since stratospheric OH is thought to carry a positive $\Delta^{17}O$ anomaly, and stratospheric $O(^3P)$ is not (Lyons, 2001), the net effect of this switch in SO_2 oxidation mechanisms would be that no $\Delta^{17}O$ anomaly can be transferred to the product sulfate (Savarino et al., 2003a).

In contrast, Bao et al. (2003), Bao (2005), and Loope et al. (2005) presented evidence from the late Oligocene ash layer from the Mid-Gering Formation in Nebraska for up to 5.8‰ positive values of $\Delta^{17}O$ in sulfate that was leached by weak acid from the ash. The ~28 Ma, pyroxene-bearing, amphibole-free mineralogical assemblage of the Gering ash was speculated to be a part of the Fish Canyon tuff (Loope et al., 2005), the largest known eruption in terms of volume of erupted material (a single 5000 km^3 eruptive unit; Lipman, 1975). Bao et al. (2003) attributed significant $\Delta^{17}O$ excesses in sulfate from Gering formation ash to the intense sulfuric "dry fog" conditions, and ozone-controlled SO_2 oxidation, following this massive Oligocene volcanic eruption. These authors found that significant positive $\Delta^{17}O$ values characterize this unit only, and are not characteristic of less voluminous ash units elsewhere, although they studied ash deposits in a number of similar semi-arid environments. The list of units without significant $\Delta^{17}O$ excursions includes voluminous ignimbrites of the Atacama desert in Chile, and those in the Antarctic Dry Valleys. Bao et al. (2003) and Bao (2005) also

reported data for ash leachates from products of several modern volcanic eruptions, notably Mt. St. Helens and Pinatubo, and observed no $\Delta^{17}O$ anomalies greater than 0.2‰. Further tests by Bao (2005) found no significant $\Delta^{17}O$ (<0.2‰) from leached atmospherically deposited sulfate in sediments from these semi-arid environments.

In contrast to the significant difference in $\Delta^{17}O$ values associated with the two eruptive events, Savarino et al. (2003b) and Baroni et al. (2007) reported mass-independent $\Delta^{33}S$ and $\Delta^{36}S$ values in ice-core sulfate from both the unknown event and the Pinatubo eruption. These observations and anomalies in fine fractions (∼sub-μm) of Northern hemisphere aerosols (Romero and Thiemens, 2003) have been interpreted to reflect stratospheric SO_2 photochemistry and similar photochemical fractionations have been observed in ultraviolet photolysis experiments with sulfur dioxide (Farquhar et al., 2000, 2001). Photochemical models have not yet been able to confirm this hypothesis, and alternative mechanisms of SO_3 photolysis for generating the non-zero $\Delta^{33}S$ and $\Delta^{36}S$ values have been proposed (Pavlov et al., 2005).

1.3. Goals of the present study

We undertook an extensive survey of sulfate from Pleistocene volcanic ash layers and their coeval proximal tephra and pumice produced by large caldera-forming eruptions in the western North America, and a series of distal and proximal historic ashes from eruptions of different magnitude around the world. We placed particular emphasis on Yellowstone's last caldera-forming eruption—the Lava Creek tuff (LCT) (Figs. 1 and 2), because its ash layers are continuously preserved and available for sampling on the North American continent and also because the effects of this "super"-eruption are being widely discussed. We have generated a dataset of all isotopes of oxygen (^{16}O, ^{17}O, and ^{18}O) and sulfur (^{32}S, ^{33}S, ^{34}S, and ^{36}S) for a subset of ash samples. Table 1 presents sulfate concentrations and its $\Delta^{17}O$, $\delta^{18}O$, $\delta^{34}S$, $\delta^{33}S$, $\delta^{36}S$, $\Delta^{33}S$, and $\Delta^{36}S$ values. We consider variations between these various isotopic parameters and their bearing on the mechanisms of SO_2 oxidation and deposition following volcanic eruptions. We also speculate on climatic effects following pre-historic large caldera forming "super"-eruptions.

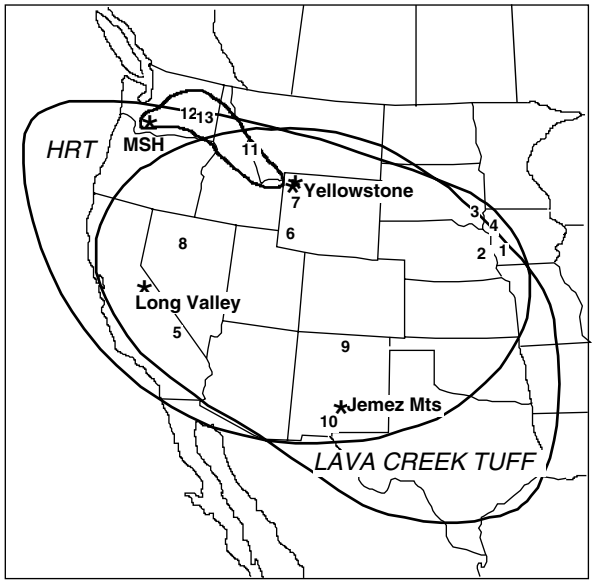

Fig. 1. Map of the North America showing source calderas, present extent of occurrence of Lava Creek tuff B ash locations, and ash from the 1980 Mt. St. Helens eruption, areas are from Izett (1981) and Sarna-Wojcicki et al. (1981, 1987). Numbers are sample localities described in Tables 1 and 2. HRT—Huckleberry Ridge tuff.

2. SAMPLES AND METHODS

2.1. Samples

Forty-four samples of volcanic ash and their enclosing sediments were collected in the field and these samples are described in Tables 1 and 2. Eighteen samples represent distal volcanic ash of Pleistocene age from the largest, caldera-forming volcanic eruptions in the western North America: the Lava Creek (LCT), Huckleberry Ridge (HRT), Bishop (BT), and Lower Bandelier tuffs (LBT) (Table 1). We have a large geographic coverage of the 0.64 Ma LCT of the last caldera forming eruption of Yellowstone spanning 2000 km from Iowa to California (Fig. 1). In most localities of these thick ash units, we collected underlying and overlying sediments to extract sulfate and measure its stable isotope ratios.

Eight historic samples of distal ash from the 1980 eruption of Mt. St. Helens, 1991 eruption of Mt. Pinatubo, eruptions of 1996 and 1998 of Iceland, and 1953 eruption of Mt. Spurr were collected during or immediately after their deposition. Most samples are fine-grained (<500 μm) distal volcanic ash that was transported by the jet stream in the upper atmosphere, but a few samples of more coarse-grained lapilli material were collected in the vicinity of the respective eruptive centers, including basaltic scoria samples from the 1996 and 1998 Icelandic eruptions deposited over the Vatnajokull glacier, and pumice from Pinatubo. All distal ash samples yielded milligram quantities of sulfate.

2.2. Methods

Sulfate is present as gypsum (Fig. 2b) and was extracted by leaching with 5% HCl and precipitated as $BaSO_4$. The barite was analyzed by the laser fluorination using methods described in detail in the Appendix A, which are similar to methods used by Bao and Thiemens (2000). The concentration of sulfate was determined by weighing the precipitated barite; repeat leaching-precipitation procedure on the same samples yielded no sulfate, suggesting that the first step leached all sulfate.

The generated gases totaling 7–20 μmol of O_2 gas were run in a dual inlet mode on Finnigan MAT 253 gas source mass-spectrometer at Caltech (Eiler and Schauble, 2004), and the University of Oregon, and masses 32, 33, 34, and 36 were recorded. The average uncertainties (standard devi-

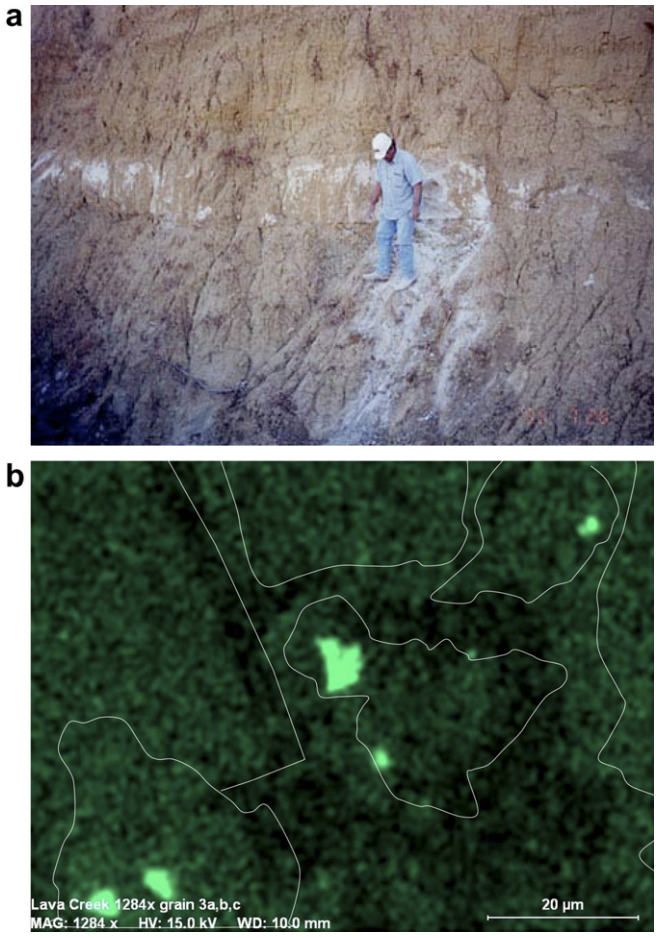

Fig. 2. Field outcrop of Lava Creek tuff B ash in easternmost Nebraska (a) deposited on glacial till and overlain by loess. (b) Gypsum particles on ash revealed by sulfur X-ray mapping and SEM imaging; sample IB04-4 of Lava Creek tuff; similar gypsum particles were imaged in Pinatubo (sample P5) and Mt. St. Helens (sample B8) ash.

ations) of extraction and analyses on $\delta^{18}O$, $\delta^{17}O$, and $\Delta^{17}O$ are 0.06‰, 0.08‰, and 0.08‰, 1 SD, respectively.

We used an ion chromatograph at the University of Oregon to check if the precipitated barite occluded any nitrate, because atmospheric nitrate has been demonstrated to possess significant $\Delta^{17}O$ anomalies (Michalski et al., 2005) and, if occluded with sulfate, can yield a false $\Delta^{17}O$ signal. Barite was redissolved in DTPA agent (Diethylene-triamine-penta-acetic acid) + NaOH following the procedure described in Bao (2006). The nitrate proportion was determined to be <2% and near detection limit for most samples (see Appendix A). Two reanalyzed samples of barite after solution-reprecipitation returned similar $\Delta^{17}O$ values (Table 1).

Sulfur isotope analyses were performed in two laboratories. The $^{34}S/^{32}S$ ratios were measured as SO_2 gas on the Delta-S mass spectrometer at the University of Nevada-Reno using automated combustion technique with uncertainty of ±0.2‰ on $\delta^{34}S$ values. Sulfur isotopic measurements of $^{33}S/^{32}S$, $^{34}S/^{32}S$, and $^{36}S/^{32}S$ ratios of 15 barite samples were performed at the University of Maryland, following their conversion to Ag_2S using published techniques (Thode et al., 1961; Forrest and Newman, 1977), and fluorination by purified F_2 gas (see Appendix A for more details). The generated SF_6 gas was purified by gas chromatography (6′–1/8″ Mol Sieve 5A column followed by a 12′–1/8″ HayeSep Q column) held at 50 °C. Purified SF_6 was introduced to a Finnigan MAT 253 dual-inlet gas-source mass spectrometer where sulfur isotope abundances were measured by monitoring the $^{32}SF_5^+$, $^{33}SF_5^+$, $^{34}SF_5^+$, and $^{36}SF_5^+$ ion beams at masses 127, 128, 129, and 131, respectively. Uncertainties associated with the sulfur isotopic measurements (0.07‰ for $\delta^{34}S$, 0.006‰ for $\Delta^{33}S$, and 0.2‰ for $\Delta^{36}S$) are taken as the standard deviation associated with long-term repeat analyses ($n = 26$) of three International Atomic Energy Association silver sulfide standards. These uncertainties reflect errors associated with fluorination and mass spectrometry procedures only.

We report our isotopic measurements as traditional δ values, where $\delta = (R_{sample}/R_{standard} - 1) * 1000$ (McKinney et al., 1950). The mass-dependent fractionation line for oxygen is defined in this work as $\delta^{17}O = 0.52 * \delta^{18}O$, and thus $\Delta^{17}O = \delta^{17}O - 0.52 * \delta^{18}O$. In the extremes of the measured $\delta^{18}O$ range, this definition gives 0 to 0.05‰ lower $\Delta^{17}O$ values than those from a power–law definition (e.g., Assonov and Brenninkmeijer, 2005): $\Delta^{17}O = \delta^{17}O - 1000 * [(1+\delta^{18}O/1000)^{0.52} - 1]$; this difference is within analytical

Table 1
Studied samples of volcanic ash, stable isotope parameters and sulfate concentration

Sample	Locality	Map Fig. 1	mg, SO_4/1 g rock	$\delta^{34}S$[a] CDT	$\delta^{18}O$ SMOW	$\Delta^{17}O$ SMOW		$\delta^{17}O$ SMOW	Deposition environment	Collected by	$\delta^{33}S$ CDT	$\delta^{34}S$[b] CDT	$\delta^{36}S$ CDT	$\Delta^{33}S$ CDT	$\Delta^{36}S$ CDT
Lava Creek tuff (0.64 Ma, 1000 km³, Yellowstone Caldera, Wyoming)															
IB04-4	Lake Tecopa, CA	5	0.61	7.8	5.97	2.26[c]	0.11	5.37	Alkaline lake	1	3.91	7.74	15.0	−0.0665	0.198
IB04-3	Lake Tecopa, CA	5	0.29	6.1	12.11	2.05[c]	0.09	8.36	Alkaline lake	1	2.96	5.90	11.5	−0.070	0.277
IB01-1	Springtown, NE	2	3.57		15.49	1.27	0.09	9.34	Fresh water lake	1	−2.41	−4.72	−9.34	0.024	−0.3854
IB01-4-3	Missouri R, IA	4	0.21		14.99	1.66	0.17	9.47	Fresh water lake	1					
IB01-1a	Glenview, IA	1	0.06		27.8	3.35	0.07	17.82	Fresh water lake	1					
IB01-3	Missouri R, IA	4	0.38		−3.78	0.05	0.08	−1.92	Fresh water lake	1	−4.47	−8.77	−17.4	0.054	−0.8216
IB04-1	Lake Tecopa, CA	5	0.24	9.2	8.80	1.56	0.08	6.14	Alkaline lake	1	4.62	9.11	17.5	−0.0673	0.139
IB01-2a	Springtown, NE	2	0.05	1.8	25.77	0.38	0.03	13.81	Fresh water lake	1	0.42	0.84	1.4	−0.0146	−0.1721
IB01-2b	Springtown, NE	2	0.05	1.8	12.06	0.97	0.07	7.26	Fresh water lake	1					
ORNA-1	Oreana, NV	8	0.94	6.0	2.29	0.42	0.09	1.61		2	3.09	6.01	11.4	0.000	−0.0284
CDH-D8836	Rio Chama, NM	9	0.26	6.2	3.69	0.83	0.09	2.75		2	3.27	6.35	12.0	0.006	−0.1259
Huckleberry Ridge tuff (2.04 Ma, 2500 km³, Yellowstone Caldera, Wyoming)															
IB04-8	Lake Tecopa, CA	5	1.36	19.8	8.54	0.76	0.06	5.21	Alkaline lake	1					
IB04-9	Alkaline lake	5	3.02	20.9	5.47	0.40	0.08	3.25	Alkaline lake	1					
Bishop tuff (0.76 Ma, 650 km³, long Valley Caldera, California)															
IB04-6	Lake Tecopa, CA	5	2.72	12.5	4.10	0.66	0.07	2.79	Alkaline lake	1					
IB04-5	Alkaline lake	5	0.05		5.54	0.80	0.05	3.69	Alkaline lake	1	6.31	12.335	23.6	−0.0261	0.027
Lower Bandelier tuff (1.61 Ma, 600 km³, New Mexico)															
TBC-1	Socorro, NM	10	0.06	8.3	11.72	0.44	0.04	6.55	Land surface	5	4.15	8.07	15.3	0.000	−0.0708
Mt. St. Helens (1980 AD, 1 km³, Washington State)															
B8	Missoula, MT	11	0.73	8.1	4.75	0.21	0.09	2.68		2	4.29	8.35	15.5	0.001	−0.4139
Davis-14	Ritzvile, WA	12	0.68	8.2	3.09	0.20	0.05	1.81		2					
Davis-12	Ritzvile, WA	13	0.39	8.6	4.45	0.21	0.10	2.53		2					
Pinatubo (1991 AD, 10 km³, Philippines)															
P5 fine	50 km away Angeles City		0.11	8.6	6.37	0.19	0.06	3.51	Roof of building	3					
P5 coarse	50 km away Angeles City		0.17	8.5	9.71	−0.04	0.05	5.02	Roof of building	3	4.33	8.46	16.1	−0.0128	−0.0638
W-1 pumice	Near volcano		0.95	5.6	8.52	0.15	0.12	4.59	Land surface	6	2.73	5.34	10.1	−0.0131	−0.0354
Mt. Spurr (1953 AD, <1 km³, Alaska)															
Mt. Spurr	1953		2.57	13.9	8.21	0.06	0.10	4.34	Roof of building	3	6.71	13.04	24.8	0.014	−0.0847
Grismvotn Caldera (1996, 1998 AD, <1 km³, Iceland)															
96 Gjalp ash	Vatnajokul glacier	Basaltic	0.08	4.5	1.33	0.03	0.04	0.72	Ice	4					
98 Gjalp ash	Vatnajokul glacier	Scoria	0.45	6.8	13.95	0.30	0.05	7.57	Ice	4	3.41	6.6096	12.5	0.008	−0.1228

Sample collected by: 1, I.N. Bindeman; 2, A.M. Sarna-Wojcicki; 3, J.H. Fournelle; 4, O. Sigmarsson; 5, P. Kyle; 6, J. Pallister.

[a] Measured as SO_2 gas.

[b] Measured as SF_6 gas.

[c] $\Delta^{17}O$ values in samples IB04-4 and IB04-3 were remeasured after barite dissolution reprecipitation in DTPA agent and yielded 2.67‰ and 2.11‰, respectively.

Table 2
Other materials and ashes that yielded little or no sulfate, or sufate with $\Delta 17O < 0.2‰$

Sample	Locality	Map position Fig. 1	Amount leached (g)	SO_4 extracted (mg)	$\delta^{34}S$	$\delta^{18}O$	$\Delta^{17}O$	±	$\delta^{17}O$	Collected by (see Table 1)
Lava Creek tuff, Yellowstone (0.64 Ma, 1000 km, Wyoming)										
LCT-3a	LCT pumice, Yellowstone	7	100	0						1
LCT-2	LCT coarse ash, Idaho	6	100	1						1
LCT-1	LCT coarse ash, Hwy 20, ID	6	100	2.3						1
Hart-1	LCT, ash, drillcore, S. Dakota	3	40	0						1
Other materials and sediments, which surround LCT										
IB04-0	Salt L.Tecopa	5	40	>200	17.9	8.87	0.20	0.07	4.82	1
IB04-13	Salton Sea salt	Near 5	40	>200	5.00	14.22	0.22	0.07	7.62	1
L-1	Hartford, S. Dakota, driillcore	3	100	0.8						1
L-2	Akron NW1 core drill core	3	100	0						1
T-1	Glacial Till, S Dakota	3	40	0						1
IB04-7	Sediments, Lake Tecopa	5	40	3.3						1
Other volcanoes and calderas										
Kurile Lake Caldera (7600 yr BP, >170 km^3, Kamchatka)										
98KAM 7.7	S Kamchatka	Kurile Lake	60	0						7
Shiveluch Volcano (1300 yr BP, >2 km^3, Kamchatka)										
SH3, Kluchi	SH3	Shiveluch	25	0						7
00K37	SH3	Shiveluch	70	0						7
Ksudach Caldera (1800 yr BP, 18 km^3, Kamchatka)										
96407/3	KS2	Ksudach	60	0						7
98KAM1.1	KS1	Ksudach	30	0						7
Fisher Caldera (9100 yr BP, >50 km^3, Alaska)										
96JF-9A	Cold Bay	Layer B	70	0						3
96AD19	Cold Bay	Layer A	90	0.74						3
8H	Cold Bay	Layer D	35	0						3
TDS566-14	Cold Bay, Alaska	Layer C	100	0						3
96JF16B	Fisher, Cold bay		35	0						3
Laki fissure (1783–4 AD, 15 km^3, Iceland)										
Laki tephra	Laki, Iceland		100	0						4
Mt. Mazama eruption (7700 BP, 50 km^3, Oregon)										
IB2005-1	Distal ash, Idaho		100	0.05						1

uncertainty of our measurements. For sulfur isotopes, we used the following expressions:

$$\Delta^{33}S = \delta^{33}S - ((\delta^{34}S/1000 + 1)^{0.515} - 1) * 1000, \quad \text{and}$$
$$\Delta^{36}S = \delta^{36}S - ((\delta^{34}S/1000 + 1)^{1.90} - 1) * 1000,$$

with constants 0.515 and 1.90 adopted from the theoretical calculations of Hulston and Thode (1965). Interpretation of small $\Delta^{33}S$ and $\Delta^{36}S$ values is of interest because different fractionation processes possess fractionation constants that may be slightly different from 0.515 or 1.90 (e.g., Young et al., 2002; Farquhar and Wing, 2003; Farquhar et al., 2003; Johnston et al., 2005; Ono et al., 2006). In order to determine the precise values of these constants for our measurements, we used a logarithmic expression to achieve linearity of the isotopic scales: $\delta^{3X}S' = \ln(\delta^{3X}S/1000 + 1)$, where X is 3, 4, or 6 for sulfur ^{33}S, ^{34}S, ^{36}S, respectively (cf. Miller, 2002; Young et al., 2002). Best-fit straight lines through these values yield net fractionation constants that characterize intrinsic fractionation due to the underlying physical or chemical process, as well as any apparent fractionation arising from mass conservation.

3. RESULTS

3.1. Depositional environments and petrography of ash layers

Except for historic samples, which were collected during or soon after the ash fall, the majority of ash falls from large Pleistocene caldera-forming eruptions are preserved as thick (50 cm to 10 m) layers in lake sediments. In most locations examined, the ash layers preserve evidence of air-fall accumulation followed by aeolian/fluvial redeposition. Examined ash layers have a sharp lower boundary, a detritus-free lower to middle part, with a sugar-white appearance. The upper half or third of the ash layer contains progressively more detrital sand or clay with color changing from white to gray and brown. The upper boundary of ash layer is typically defined, but the overlying sediments contain 10% of ash from the ash horizon.

The depositional environments (Table 1) range from present dry and arid conditions in alkaline Lake Tecopa in California near Death Valley (Nelson et al., 2001), to presumably fresh-water synglacial lakes in Iowa, Nebraska, and S. Dakota, where ash layers are interpreted to represent lacustrine sediments in ice-dammed lakes along the Missouri River Valley embedded into the glacial till (Bettis, 1990; Bettis et al., 2003; A. Bettis, personal communication 2001). In these states, the Lava Creek tuff generally occurs as a layer within glacial till and loess.

In New Mexico, Lava Creek ash bed is enclosed in high river terrace sediments. The alkaline lake Tecopa in California existed as a lake of variable extent throughout the Pleistocene and 20% of its lacustrine sediment column is represented by the volcanic ash of different age, ranging from Huckleberry Ridge tuff (2.04 Ma) to 0.64 Ma Lava Creek tuff (e.g., Larsen et al., 2001).

Petrographic examination of ash was performed under the binocular and polarizing microscopes. In distal Yellowstone ashes, phenocrysts are very scarce and the material is represented by 99% pure and fresh (isotropic), to slightly devitrified (1–2%) to spherulitic ash. Major element chemical analyses of selected bulk samples of distal and proximal Yellowstone ashes are given in Table A (internet repository). Comparison of these ashes with proximal samples and with the LCT tephrochronological standard confirms their fresh unaltered nature.

Extensive secondary electron imaging and electron microprobe analysis has previously been performed on ash particles in Lava Creek, Bishop, Huckleberry Ridge, and Lower Bandelier tuffs (Sarna-Wojcicki et al., 1987), but sulfate concentration and mode of occurrence has not been studied. We performed secondary and backscattered electron imaging and sulfur X-ray mapping using a variable pressure SEM at the University of Oregon to image sizes and textural positions of sulfate in ash samples (Fig. 2b). We found that sulfate occurs as 1–10 μm gypsum particles scattered on the surface of ash. We also imaged similar gypsum particles on the surfaces of historic Pinatubo and Mt. St. Helens distant ash particles (samples P5 and B8, Table 1). In studies of Bao et al. (2003) and Loope et al. (2005) sulfate is present as admixture to the carbonate cement of volcanic ash.

3.2. Sulfate concentration and its $\delta^{18}O$, $\delta^{34}S$, and $\Delta^{17}O$ values

Tables 1 and 2 present data on extracted quantities of sulfate from ash layers and their country rocks. Additionally, the second part of Table 2 presents data on thin distal volcanic ash layers from wet climate environments of Iceland, Kamchatka, and Alaska which were also studied, but for which the amount of sulfate extracted was either nil or too low (<0.05 mg/g) to perform an isotopic analysis. The majority of ash samples that were deposited in lake sediments yielded significant quantities of sulfate during leaching (Table 1), except for one thin layer of Lava Creek tuff (Hartford ash) from South Dakota drillcore that was deposited between loess and till; this sample of ash and surrounding loesses did not yield any sulfate (Table 2).

Acid leaching-extraction tests were undertaken to evaluate whether these enclosing sediments and salts contain significant sulfate concentration of non-volcanic origin, and if they do, what is the oxygen isotope ratios of this sulfate. The extraction yielded no sulfate in sediment samples in the immediate vicinity of the ash bed in either tills or loess from Nebraska and Iowa localities. Among four lacustrine shale sediments in Lake Tecopa, three of which yielded no sulfate, only shale from the lake sediment between the layers of 0.76 Ma Bishop tuff and 0.64 Ma Lava Creek tuff ash beds contained a little sulfate (sample IB04-7, Table 2). This was is in sharp contrast to the abundant sulfate in ash beds themselves (Table 1). However, the salt on the surface of presently dry lake Tecopa, contained significant quantities of sulfate but with only modest positive $\Delta^{17}O = 0.2‰$. This surface sulfate likely has a mixed origin, with a significant proportion coming from the present lake Tecopa watershed area (Larsen et al., 2001) and some from subsurface leaching of sulfate from the underlying ash beds and sediments with significant $\Delta^{17}O$ excesses. Salts and waters in the

southwestern USA and in the Death Valley region in particular, have $\Delta^{17}O$ near 0; only surface varnishes resulting from atmospheric aerosol deposition yields modest (<0.5‰) $\Delta^{17}O$ anomalies in this desert region (Bao et al., 2001).

Thus, only ash layers in our study yielded significant quantities of sulfate with variable but high $\Delta^{17}O$ values. The concentration of acid-soluble SO_4^{2-} typically range from 100 to 3000 ppm (Table 1), which encompasses concentration of sulfate released by the corresponding volcanic eruptions: the Bishop (1740 ppm SO_4/1 g of magma), Pinatubo (2400 ppm), and Mt. St. Helens (1200 ppm) eruptions (estimated from Wallace, 2003). If these estimated values are indicative of the entire eruptive event, ash samples at the lower end of our measured range may have been lost sulfate to the environment after deposition. However, sulfate occurs in ash layers quite inhomogeneously: single Pleistocene ash layers may exhibit a significant range (e.g., 0.05–2.72 mg/g within a 1.5 m thick layer of Bishop tuff) and the same is true for the historic ash samples: e.g., Pinatubo (0.11–0.95). Initial variations in sulfate concentrations due to scavenging effects in the volcanic plume (e.g., Gerlach and McGee, 1994; Rose, 1977), and/or redistribution within ash layer after its deposition may also explain these differences in concentration. The postdepositional redistribution process should have minimal effects on stable isotope composition of $\delta^{34}S$ and $\delta^{18}O$ as is seen in Table 1 and noted by others (Vanstempvoort and Krouse, 1994; Khademi et al., 1997; Bao, 2005), but should not measurably change $\Delta^{17}O$, $\Delta^{33}S$, or $\Delta^{36}S$. We suggest, therefore, that the measurements in our global dataset reflect differences in the time-integrated amount of sulfate accumulated during the transport and subaerial residence of a particular ash parcel, before being buried and isolated from the atmosphere by the overlying sediments.

3.3. Stable isotopes by eruption

Table 1 and Figs. 3–9 present stable isotopic parameters measured on sulfate ash leachates of this work. Our stable isotope results can be compared with those from Bao et al. (2003) and Savarino et al. (2003a,b) for the same eruptions of Pinatubo and Mt. St. Helens, and demonstrate that $\delta^{34}S$ and $\delta^{18}O$ values of our and their studies overlap and are in the expected range for the magmatic SO_2 gas. This suggests consistency of sulfate leached from ash by weak HCl acid and subsequent fluorination techniques used by us and Bao et al. (2003), and compatibility of this analytical

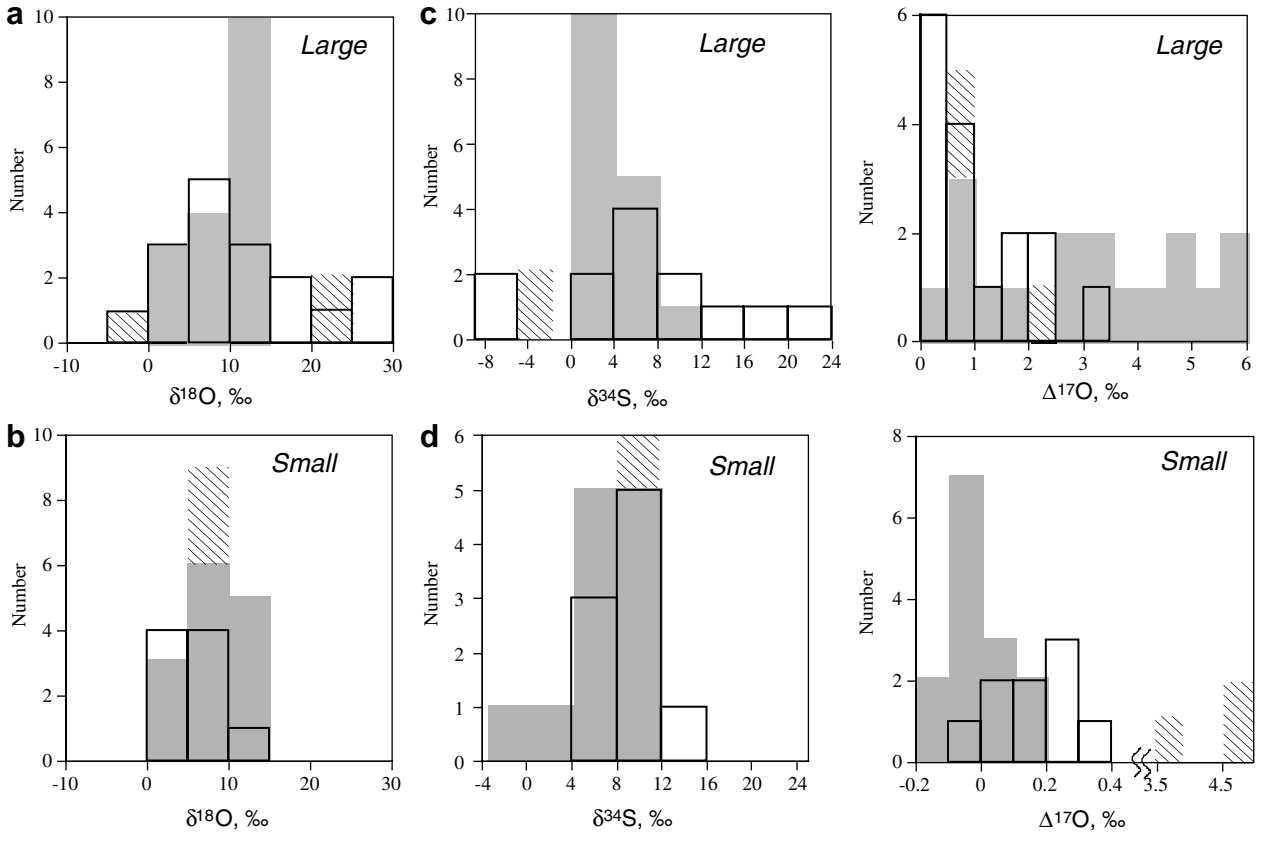

Fig. 3. Histograms of $\delta^{18}O$, $\Delta^{17}O$, and $\delta^{34}S$ values of leachates from volcanic ash. Comparison of isotopic parameters in sulfate in large (>500 km^3 of magma) vs. medium and small (<15 km^3 of magma) volcanic eruptions. Results of this work are shown by thick lines. Data from Bao et al. (2003) for a voluminous Oligocene ash layer in Nebraska and smaller volume modern ashes are shown in shadowed pattern. Data from Savarino et al. (2003a,b) on isotope analysis of Antarctic ice cores are shown by hatched pattern. Notice the significant range in each parameter, greater range for large eruptions, and more significant overall $\Delta^{17}O$ enrichment in the products of the large eruptions.

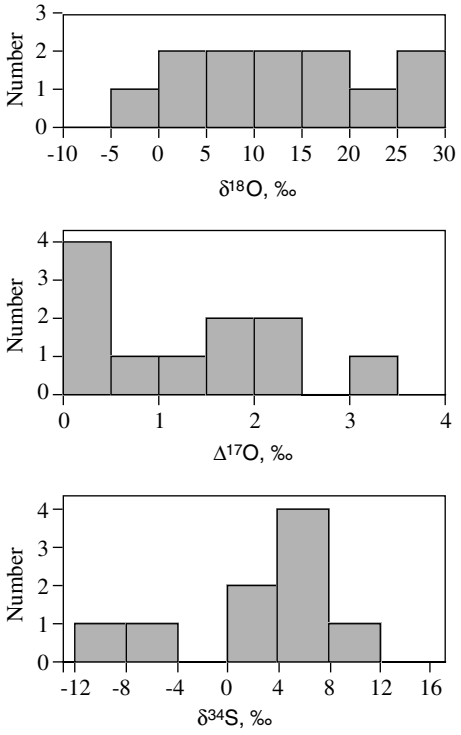

Fig. 4. Histograms of $\delta^{18}O$, $\Delta^{17}O$, and $\delta^{34}S$ values of leachates from a single eruption—the Lava Creek tuff of Yellowstone. Sample localities are widespread and are shown on Fig. 1. Notice that values of $\delta^{18}O$ and $\Delta^{17}O$ spread over a significant range, while variation in $\delta^{34}S$ is more subdued and is in the general range of magmatic gases. The spread is interpreted to represent atmospheric oxidation of volcanic SO_2 gas by high $\delta^{18}O$ and $\Delta^{17}O$ gases such as ozone, H_2O_2 and OH, followed by formation of H_2SO_4 aerosols, followed by Rayleigh distillation during rainout.

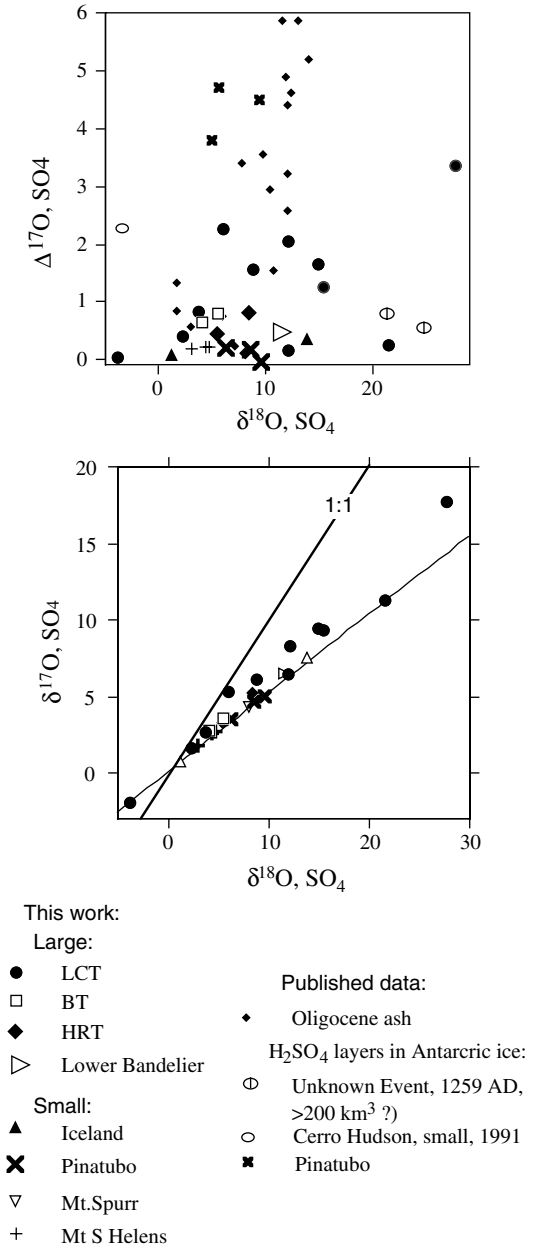

Fig. 5. The $\delta^{18}O$ vs. $\delta^{17}O$ and $\Delta^{17}O$ vs. $\delta^{18}O$ in sulfate. Oligocene ash is from Bao et al. (2003); H_2SO_4 data from Antarctic core is from Savarino et al. (2003a). With increases in $\delta^{18}O$, the positive departure from the terrestrial mass fractionation line increases. The slope of this increase is seen as being variable for each eruption. For example, compare steeper slope for large volume Oligocene eruption with the data of the present paper for the Lava Creek tuff of Yellowstone. This difference may reflect Rayleigh distillation during transport and rainout for each particular eruption.

method to those used by Savarino et al. (2003a,b) in their different study of H_2SO_4 in Antarctic ice. Note that fractionations due to differences in extraction and analysis are mass-dependent processes and should not measurably change the $\Delta^{17}O$, $\Delta^{33}S$, or $\Delta^{36}S$.

3.3.1. Global data set

In our dataset, there is significant variation in O and S isotopes: value of $\delta^{34}S$ vary by 29‰, $\delta^{18}O$ by 30‰, and $\Delta^{17}O$ by 3.3‰. Variations in $\Delta^{33}S$ and $\Delta^{36}S$ are small and adhere to mass-dependent behavior (Table 1). When products of all eruptions are considered together, there appears to be a weak negative correlation between $\delta^{34}S$ and $\delta^{18}O$ but no apparent correlation between $\delta^{34}S$ and $\Delta^{17}O$ (Figs. 6a and b). Collectively, products of small (ca. <1 km^3) to medium-scale (ca. 10 km^3) eruptions are characterized by a significant isotopic range, whereas variations among three samples of each 1980 Mt. St. Helens and 1991 Mt. Pinatubo eruptions span only a few permil in $\delta^{34}S$ and $\delta^{18}O$, and have $\Delta^{17}O < 0.2$‰. Products of a single supereruption—the Lava Creek tuff—exhibit most of the described isotopic range (Fig. 4). Collectively, products of four large caldera-forming eruptions, dominated by the dataset of the Lava Creek tuff, span a far greater range in O and S stable isotope values compared to the small to medium-scale eruptions.

A three-isotope oxygen plot emphasizes the extent of deviation from the terrestrial mass-fractionation line (Fig. 5) with the LCT accounting for the largest $\Delta^{17}O$

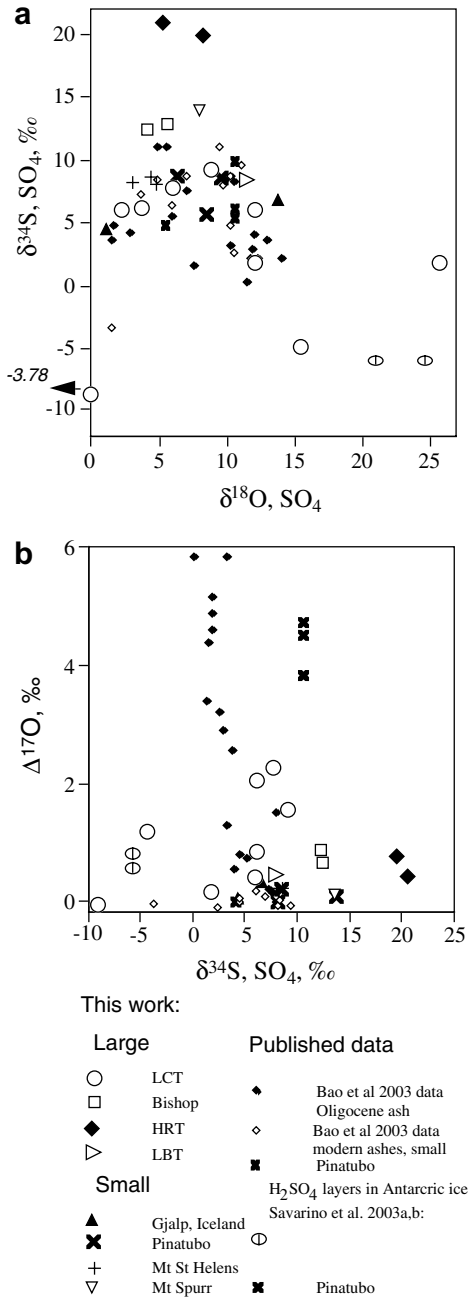

Fig. 6. $\delta^{18}O$ vs. $\Delta^{17}O$ vs. $\delta^{34}S$ values in sulfate from volcanic ash. (a) $\delta^{18}O$ vs. $\delta^{34}S$ plots measured (this work) and published ranges of oxygen and sulfur isotopic measurements, which demonstrate significant ranges, scatter, and decoupling of variations in sulfur and oxygen isotopes. (b) $\Delta^{17}O$ vs. $\delta^{34}S$ plots measurements of this work and published data. Our data demonstrates subtle positive correlation of these parameters and for the Lava Creek tuff in particular. Data of Bao et al. (2003) for a single voluminous ash layer in Nebraska shows subtle negative correlation. Pinatubo data (this work, Bao et al., 2003; Savarino et al., 2003a,b) shows subtle positive correlation. Apparent positive and negative variations may results from specifics of Rayleigh distillation during transport and rainout for each particular eruption.

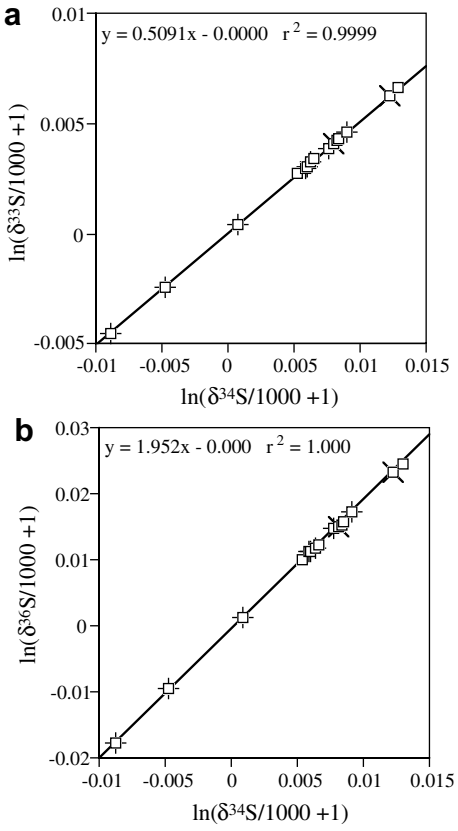

Fig. 7. Rare sulfur isotopic ratios in sulfate from volcanic ash. $\delta^{34}S$ vs. $\delta^{33}S$ (a), and $\delta^{34}S$ vs. $\delta^{36}S$ (b) expressed as logarithms that define slopes of 0.509 and 1.95 respectively. Regressed slopes are based on Lava Creek tuff data (+) and two other large caldera forming eruptions (X), see Table 3 for calculated slopes for each dataset.

range. The data plot to the right of a line which defines mixing between components belonging to the line with the slope of ~0.5 and those with the slope of 1 (e.g., ozone). The slope of $\Delta^{17}O$ vs. $\delta^{18}O$ dependence determined in this work plots in the middle of those determined in two previous studies (Bao et al., 2003; Savarino et al., 2003a). The slope is steep in the study of Bao et al. (2003) for the 28 Ma Mid-Gering eruptive unit, but the data on H_2SO_4 in Antarctic ice of Savarino et al. (2003a) define both steep (for Pinatubo) and shallow (for the unknown 1259 AD eruption) slopes in $\Delta^{17}O$ vs. $\delta^{18}O$ coordinates.

Overall, sulfur isotopic compositions are consistent with mass-dependent fractionation (Fig. 7–9, Table 3). Variations in slopes of $\delta^{33}S'$ vs. $\delta^{34}S'$, and $\delta^{36}S'$ vs. $\delta^{34}S'$ (see end of Section 2 for definitions) for the global dataset of small eruptions cluster within analytical uncertainty around equilibrium isotopic fractionation lines with the slopes of 0.515 and 1.90, respectively (cf. Fig. 3 in Farquhar and Wing, 2003). However, data for large caldera-forming eruptions, dominated heavily by the dataset of Lava Creek tuff of Yellowstone, are significantly different (Table 3). These data are consistent with either Rayleigh isotope distillation processes, or non-equilibrium (kinetic) mass-dependent fractionation (Table 3). The isotopic variations in these

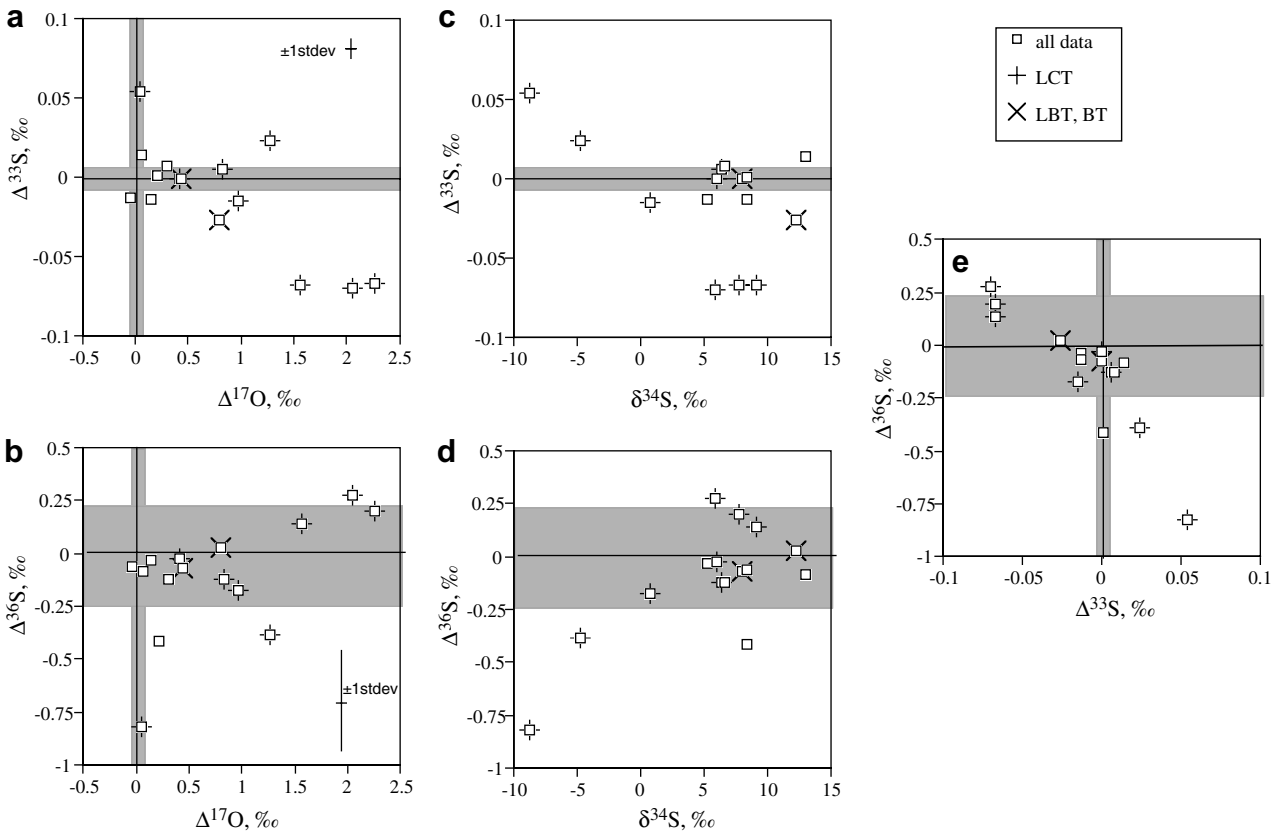

Fig. 8. Isotopic fractionation on three isotope plots: (a) $\Delta^{33}S$ vs. $\Delta^{17}O$; (b) $\Delta^{36}S$ vs. $\Delta^{17}O$; (c) $\Delta^{33}S$ vs. $\delta^{34}S$; (d) $\Delta^{36}S$ vs. $\delta^{34}S$; and (e) $\Delta^{36}S$ vs. $\Delta^{33}S$. Gray fields denote ±1 SD of measurements, vertical and horizontal lines indicate fractionations with exponents of 0.515 for $\delta^{33}S$ and $\delta^{34}S$ and 1.90 for $\delta^{36}S$ and $\delta^{34}S$. LCT, Lava Creek tuff; LBT, Lower Bandelier tuff; BT, Bishop tuff (see Tables 1 and 2 for data).

subsets are further described below and plotted on Fig. 9 vs. $\delta^{34}S$, $\Delta^{17}O$, and $\delta^{18}O$ values.

3.3.2. Pinatubo

Our $\delta^{18}O$ values for proximal and distal samples of the 1991 eruption are comparable to a datum from Bao et al. (2003), and three data points of Savarino et al. (2003a) and within the expected primary magmatic range of 6–9‰. However, while our data and the datum of Bao et al. (2003) shows $\Delta^{17}O$ near zero, the data of Savarino et al. (2003a) indicate much larger $\Delta^{17}O$ values of 3.5–4.8‰.

Our $\delta^{34}S$ values of leached sulfate (Table 1, Fig. 6a) span from 5.6‰ (large proximal pumice) to 8.6‰ for the ash deposited 50 km away in the city of Angeles. Fournelle et al. (1996) reported a 8.2‰ $\delta^{34}S$ value for magmatic sulfate, and McKibben et al. (1996) used SHRIMP ion probe analysis to determine a 5–11‰ $\delta^{34}S$ range in individual anhydrite crystals and estimated primary equilibrium SO_2 gas values in the 5–7‰ range. Savarino et al. (2003a,b) reported $\delta^{34}S$ value of 10.9‰ for Pinatubo sulfate in Antarctic ice. Thus, the reported values of $\delta^{34}S$ and $\delta^{18}O$ of sulfate from the 1991 Pinatubo eruption show a 5–0‰ range for both isotopes, as determined by four labs for samples collected 15,000 km apart between the center of the eruption and the South Pole. Still this is a relatively narrow range as compared to the Lava Creek, or Mid-Gering ash beds (Fig. 6a).

Total sulfur isotopic ratios measured by us in two Pinatubo samples do not possess mass-independent signatures (Table 1). The slopes of $\delta^{33}S'$ vs. $\delta^{34}S'$ and $\delta^{36}S'$ vs. $\delta^{34}S'$ are 0.515 and 1.89 (Fig. 9), which are consistent with equilibrium-type mass-dependent fractionation (see below). This is in contrast to the anomalous sulfur isotopic compositions in ice-core sulfate attributed to the Pinatubo eruption (Savarino et al., 2003b).

3.3.3. Other small modern eruptions

Small modern eruptions such as Mt. St. Helens, Mt. Spurr, and two eruptions in Iceland, exhibit a narrow but diverse range of stable isotopic compositions, and invariably small, but recognizable $\Delta^{17}O$ in the range <0.3‰. In particular, three samples of Mt. St. Helens yielded consistent 0.21‰ values while the 1998 eruption in Iceland yielded 0.3‰, which is significantly different from 0 based on the uncertainty of our standards. Sulfur isotope ratios from these samples define slopes consistent with equilibrium isotopic fractionation (Table 3).

3.3.4. Lava Creek tuff and other large eruptions

The sulfate in the ash from the youngest caldera-forming eruption of Yellowstone covers much of the isotopic range of all other eruptions combined (Table 1; Fig. 4), and it is important to note that the isotopic variations seen in this

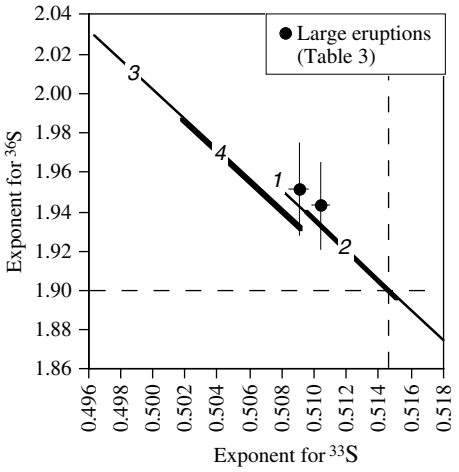

Fig. 9. Slopes of sulfur isotope fractionations calculated for individual samples spanning the entire range from kinetic to equilibrium (Table 3). Lines labeled 1 and 2 are Rayleigh distillation slopes for one step and two step SO_2 oxidation, respectively, using a network approach similar to that described in Farquhar et al. (2003); lines 3 and 4 are kinetic isotope fractionation with kinetic and reduced masses, respectively, using Young et al. (2002) formulations. Dashed lines indicate expected values for equilibrium isotope fractionation of 0.5145 and 1.90. Notice that products of Lava Creek tuff eruptions cluster around non-equilibrium fractionation trends (Rayleigh or kinetic), while data for most small eruptions agree with or deviate slightly from the equilibrium isotope fractionation (Table 3).

unit largely coincides with global data set for eruptions of similar magnitude (i.e., BT, HRT, and LBT). In particular, $\Delta^{17}O$ correlates positively with $\delta^{18}O$ (Fig. 5), but exhibits no correlation with $\delta^{34}S$ (Fig. 6b); whereas $\delta^{18}O$ and $\delta^{34}S$ exhibit a negative correlation. Plotting data from Table 1 results in no dependence of either of the stable isotope parameters, nor sulfate concentration, on location (e.g., Iowa-Nebraska vs. California), depositional environment (alkaline Lake Tecopa vs. synglacial ice-dammed lakes), or the distance from the eruption center. Most of the studied samples are located many hundreds of kilometers away from Yellowstone, and this distance alone suggests stratospheric jet-stream transport. Because these distal ash particles contain sulfate with large $\Delta^{17}O$ anomalies, it additionally suggests stratospheric reactions with high-$\Delta^{17}O$ compounds.

The $\delta^{34}S$ values of LCT samples range from −9‰ to +9‰, and do not exhibit mass-independent sulfur behavior relative to their associated $\delta^{33}S$ values (Tables 1 and 3; Fig. 7–9). Slopes of $\delta^{33}S'$ vs. $\delta^{34}S'$ and $\delta^{36}S'$ vs. $\delta^{34}S'$ regressed through eight data points define values of 0.509 and 1.95 (Table 3). These slopes are inconsistent with those calculated for intrinsic equilibrium isotope effects (Hulston and Thode, 1965; Farquhar and Wing, 2003), and resemble values associated with either Rayleigh or non-equilibrium isotope effects (Table 3 and Fig. 9).

Similarly, other large volcanic eruptions: BT, LBT, and HRT all possess significant non-zero $\Delta^{17}O$ values that exceeds that of small eruptions, and lack mass-independent sulfur isotopic signatures. We discuss the implications of these results below.

4. DISCUSSION

The discussion below addresses the following results of the present work: (1) the origin of significant isotopic ranges of $\delta^{34}S$ and $\delta^{18}O$ of volcanic sulfate; (2) the origin of mass-independent variations in oxygen within products of large caldera-forming eruptions; (3) the origin of mass-dependent sulfur isotope fractionation via kinetic or Rayleigh sulfate removal processes; and (4) discussion of these results in the framework of published data. The common theme behind these interpretations is the sudden volcanic release of variable quantities of SO_2 gas followed by its oxidation to SO_3 and eventual precipitation as H_2SO_4.

4.1. $\delta^{34}S$ values of SO_2 gas after rapid release in volcanic eruptions

Sulfur isotopic measurements in the present study suggest that SO_2 gas was not affected by direct photolysis and that the isotopic composition of the sulfate was set primarily by mass-dependent chemical reactions involving oxidation of SO_2. Sulfur isotopic variations during SO_2 oxidation into sulfuric acid following volcanic eruptions has been described in terms of equilibrium, Rayleigh, and gas-phase non-equilibrium processes occurring at different altitudes. These processes involve reactions in volcanic plume, troposphere, and stratosphere, aqueous- and gas-phase reactions (Castleman et al., 1973; Ohmoto and Rye, 1979; Leung et al., 2001).

After separation from sulfur-bearing magma, the dominant SO_2 gas, and minor H_2S are oxidized to H_2SO_4 which,

Table 3
Slopes of mass-dependent sulfur isotopic variations for different subsets of data

Eruptive unit	$\ln(^{33}S/^{32}S)/\ln(^{34}S/^{32}S)$	$\ln(^{36}S/^{32}S)/\ln(^{34}S/^{32}S)$	Ranges			
			n	$\delta^{18}O$ (‰)	$\delta^{34}S$ (‰)	$\Delta^{17}O$
Lava Creek tuff	0.5091	1.952	8	30	18	3.3
Large caldera-forming eruptions	0.5105	1.943	10	32	30	3.3
Pinatubo 1991	0.5151	1.890	2	3.3	3.0	0.2
All Holocene eruptions	0.5177	1.898	5	12.6	9.4	0.3
All data	0.5120	1.933	15	32	30	3.3
Equilibrium fractionation[a]	0.515	1.90				
Kinetic fractionation[b]	0.508	1.96				

[a] Equilibrium fractionation, calculated using reciprocal atomic masses (e.g., Hulston and Thode, 1965).
[b] Kinetic isotope fractionation calculated using reduced molecular masses of SO_2 gas (e.g., Young et al., 2002).

at equilibrium, would be strongly enriched (>10‰ and >50‰, respectively) in ^{34}S relative to gaseous SO_2 and H_2S (e.g., Ohmoto and Rye, 1979; Taylor, 1986). The sulfuric acid has very low vapor pressure and may be present as micron-scale solid particles that precipitate quickly (days to weeks) on the ground after eruption. In aqueous conditions, equilibrium SO_2 oxidation will generate $\delta^{34}S$ values of the sulfuric acid and subsequently sulfate that are significantly higher than the original SO_2 gas of the volcanic plume (e.g., >8–10‰, Ohmoto and Rye, 1979). Thus, first precipitation from a cloud of H_2SO_4 is expected to have high $\delta^{34}S$ values, but with depletion of overall S in the cloud, the $\delta^{34}S$ of the remaining H_2SO_4 could become strongly negative. A simple Rayleigh mass balance calculation shows that at constant temperature of 25 °C and $\Delta SO_4aq–SO_2$ gas of +12‰ (Sakai, 1968), the first H_2SO_4 droplets will be +13‰ ($f = 0$), +10 ($f = 0.75$), +5‰ ($f = 0.5$), −4‰ ($f = 0.25$), and −23‰ ($f = 0.05$), if the initial $\delta^{34}S_{SO_2}$ were +1‰, where f is the fraction of SO_2 gas remaining. Thus, Rayleigh distillation in the aqueous phase within a rising volcanic plume is capable of causing a >30‰ variation in $\delta^{34}S$ values, and a progressive decrease in $\delta^{34}S_{Sulfate}$ values of precipitation from a volcanic plume. This process may be most effective in the *troposphere*, where an effectively infinite source of water is available, or initially in the water-rich volcanic plume itself before it freezes out during adiabatic assent.

However, non-equilibrium isotope effects in homogeneous gas-phase reactions and in heterogeneous reactions on the surfaces of aerosol particles may mostly control isotopic evolution during SO_2 oxidation in the water-depleted stratosphere. It has been suggested that more than half of SO_2 oxidation in the stratosphere proceeds by the homogeneous oxidation in the gas phase and involves the following sequence of reactions (Fulle et al., 1999):

$$SO_2 + OH + M = HOSO_2 + M$$
$$HOSO_2 + O_2 = HO_2 + SO_3$$
$$SO_3 + 2H_2O = H_2SO_4 \cdot H_2O$$

The unimolecular reaction model of Leung et al. (2001) predicts that this gas phase SO_2 oxidation pathway is controlled by reaction with the OH radical, and that $^{34}SO_2$ reacts faster with OH than $^{32}SO_2$. This step has an extremely large inverse kinetic isotope effect, with fractionation factors in 1.10–1.16 range (100–160‰) under relevant lower stratospheric/upper tropospheric pressures and temperatures (Leung et al., 2001).

Consistent with the treatment of Leung et al. (2001) are the observations of Castleman et al. (1973). These authors studied $\delta^{34}S$ and total SO_4^{2-} concentration of stratospheric aerosols at 19 km altitude following the massive 1963 Agung eruption in Bali, Indonesia. These authors noted that soon after the eruption, stratospheric $\delta^{34}S$ values were close to magmatic (+2‰ to +5‰). In 100 days both parameters peaked and $\delta^{34}S$ was +20‰, however, after 500–800 days, the sulfate concentration and its $\delta^{34}S$ values exhibited steady decline down to −24‰, before slowly recovering to the background level of +2.6‰. The homogeneous gas phase oxidation by the OH radical in the stratosphere (Leung et al., 2001; Leung, 2003) models these variations, and the kinetics of the OH radical oxidation explains the magnitude, the sequence and excursions of concentrations and its $\delta^{34}S$ value when combined with Rayleigh removal of the reaction product H_2SO_4.

Therefore, for sulfur isotopes, a gas-phase non-equilibrium reaction model can produce significant isotopic variation during SO_2 oxidation. However, a heterogeneous oxidation pathway is likely to be important (Fulle et al., 2001) and probably includes a number of reactive steps in which local equilibrium is established. Since there is a finite amount of SO_2 in the volcanic plume, a Rayleigh component may be involved in the isotopic fractionation as well. Stratospheric observations indicate a 30‰ range in $\delta^{34}S$ during the course of volcanic eruption of SO_2 and its subsequent oxidation over multiple years. Accordingly, the large $\Delta^{17}O$ anomaly, ca. 29‰ range in $\delta^{34}S$ seen among our global data set (e.g., Fig. 6), and also in the products of a single eruption—the Lava Creek tuff—is interpreted to reflect primarily stratospheric processing, and we use rare sulfur isotopic measurements below to shed light onto this possibility.

4.2. $\Delta^{17}O$ and $\delta^{18}O$ values of sulfate aerosols

The discovery of a mass-independent isotope signature in oxygen from ash-derived sulfate suggests that photochemically produced components such as high-$\delta^{18}O$, high-$\Delta^{17}O$ ozone should either be directly involved in oxidation (Lee et al., 2001), or be involved in the chain of reactions that produce mass-independent OH radicals (Lyons, 2001). We infer that interaction with tropospheric water was limited because this should have erased the mass-independent isotopic signature (Lyons, 2001). The large $\Delta^{17}O$ signal implies that the SO_2 oxidation reactions involved compounds that originated in the stratosphere.

Globally, one half of SO_2 is oxidized to H_2SO_4 by heterogeneous aqueous oxidation, and the other half through the gas phase reactions (Finlayson-Pitts and Pitts, 2000). If volcanic SO_2 oxidation involved only heterogeneous aqueous oxidation and proceeded via hydrogen peroxide or ozone (Tanaka et al., 1994), both high-$\delta^{18}O$ and high-$\Delta^{17}O$ compounds, then a positive correlation of $\delta^{18}O$ vs. $\delta^{34}S$ and $\Delta^{17}O$ vs. $\delta^{34}S$ would be expected. If the homogeneous gas-phase oxidation model by OH of Leung (2003) and Lyons (2001) is taken as a guide for both sulfur and oxygen isotopes, then it may explain negative $\delta^{18}O$ vs. $\delta^{34}S$ isotope correlation that is seen in products of large caldera forming eruptions of the same magnitude: LCT, BT, HRT, and LBT (Fig. 6a).

Nonetheless, $\Delta^{17}O$ values >2‰ in our dataset and those of Bao et al. (2003) and Savarino et al. (2003a) suggest that it is ozone and direct products of its breakdown, the highest $\Delta^{17}O$ compounds, that exerts a major control on the isotopic evolution of sulfate oxygen in the SO_2 oxidative pathway. While the $\delta^{18}O$ values of ozone are variably high (ca. +25–50‰), the stratospheric and upper tropospheric water is extremely depleted in $\delta^{18}O$ due the to freeze out effects and due to methane oxidation (ca. −100‰ to −250‰, Bechtel and Zahn, 2003; Webster and Heymsfield, 2003). As a result, the overall oxygen isotope fractionation during SO_2 oxidation are likely to be highly variable, as illustrated by the ~30‰ range in $\delta^{18}O$ values in our data set (Fig. 6).

In conclusion, decoupled variations between sulfur and oxygen isotopes is expected because of different photochemical reactions of oxygen and sulfur in SO_2, and subsequent isotopic fractionation during oxidative chemistry and Rayleigh processing.

4.3. Ozone layer response to introduction of gigaton quantities of SO_2

The presence of a the mass-independent (MIF) signature in the final product sulfate associated with volcanic ash deposits suggests that introduction of large quantities of SO_2 and ash into the stratosphere consumes ozone that can be scaled with the volume of the eruption. If the overall oxidation reaction net is written as:

$$SO_2 + \{OH^* \text{ or } O(1D)^*\} + H_2O = H_2SO_4^*$$

where * denotes the MIF ^{17}O signature carried by ozone-derived radicals (e.g., Lyons, 2001), only one out of four oxygen atoms in H_2SO_4 originates from a mass-independent source.

If stratospheric ozone is taken to have $\Delta^{17}O = 32 \pm 10‰$ (e.g., Krankowsky et al., 2000), and the same or similar $\Delta^{17}O$ characterizes its reaction products (e.g., Lyons, 2001), then the maximum achievable $\Delta^{17}O$ of sulfate is ~8‰. The prevalent 2–3‰ $\Delta^{17}O$ signal found in our dataset for the Lava Creek tuff suggests that the sulfate-forming reaction with stratospheric ozone has an efficiency factor of ~0.3–0.4. This efficiency factor incorporates both the effect of plume-associated SO_2 getting oxidized through a non-MIF pathway and the possibility of dilution from non-plume associated sulfate that does not bear a MIF signature. Alternatively, a dilution factor plays a role, in which, for example, a comparable amount of tropospherically oxidized SO_2 without MIF signature is admixed with stratospheric sulfate with $\Delta^{17}O$ ~8‰. Values of up to $\Delta^{17}O = 6‰$ reported by Bao et al. (2003) may suggest greater reaction efficiency (or less dilution) in the Mid Gering ash bed.

An ~33% reaction efficiency or dilution ratio translates into $\sim 1 \times 10^{13}$ mol of O_3 consumed by a 2 Gt (3.12×10^{13} mol) SO_2 eruption; under the static assumption of no increase or decrease in ozone production, this corresponds to 15% reduction in the overall ozone mass ($\sim 7 \times 10^{13}$ mol as calculated from 300 Dobson units times Earth's surface area). Greater $\Delta^{17}O$ values from the Mid Gering ash bed may correspond to larger SO_2 releases, and an overall ozone mass be reduced by up to in half. Moreover, after the volcanic eruption the entire mass of SO_2 is initially confined to a certain latitudinal band for days to weeks. Reprocessing of the volcanic SO_2 during transport through the same ozone mass may lead to the eventual exhaustion of ozone at that latitude.

It is not immediately obvious, however, what effect this interaction may have on UV fluxes leaving the stratosphere or on the water budget of the stratosphere. The destruction of ozone may not immediately lead to an increased UV flux on the ground because SO_2 absorbs UV radiation at comparable wavelengths (Finlayson-Pitts and Pitts, 2000). The production of reflective sulfate aerosols may occur rapidly to compensate for the overall reduction in both SO_2 and ozone. However, halogens and fluorocarbons absorbed on the aerosol particles may catalyze ozone destruction (e.g., Brasseur and Granier 1992; Solomon 1999). The overall oxidation reaction also consumes water in mole-for-mole proportions with SO_2. However, water is the dominant volatile in a volcanic plume and, counterintuitively, stratospheric eruptions may lead to the watering of the stratosphere (A. Robock, pers. comm., 2006) if the amount of injected water is in excess of that consumed by reaction with SO_2.

4.4. Total sulfur isotopic parameters of sulfate aerosols

Our data do not expand the list of modern sulfates that possess mass-independent $\Delta^{33}S$ and $\Delta^{36}S$ (cf. Romero and Thiemens, 2003; Savarino et al., 2003b), nor does it confirm suggestions that Archean supereruptions were capable of causing MIF of S (e.g., Ohmoto et al., 2006). This has several potential implications. First, the SO_2 oxidation reactions recorded in our sulfate dataset apparently did not involve significant photolysis of SO_2, a process that has been proposed to explain anomalous sulfur isotopic fractionation in early Earth's record (Farquhar et al., 2001). This is contrary to our starting hypothesis that larger eruptions with higher-altitude plumes (Textor et al., 2003) may be associated with SO_2 photolysis driven by exposure to ultraviolet radiation <300 nm, and, thus, these higher-altitude plumes were expected to show a greater proportion of non-mass-dependent sulfur isotope effects. Second, although the lack of anomalous sulfur isotope fractionation has been used to rule out a stratospheric source for ice-core sulfate (e.g., Alexander et al., 2003), our results suggest that care should be taken in applying this characteristic to sulfate associated with Plinian volcanic eruptions. Volcanological evidence implies that at least some of the eruptions we investigated must have pierced the stratosphere, yet we found no anomalous sulfur isotopic fractionation in our samples (Table 1). Third, oxidation of most SO_2 from stratospheric volcanic injections is generally taken to result from gas-phase reaction with stratospheric OH (e.g., Fulle et al., 1999). A lack of sulfur isotope anomalies in our sample set suggests that none of the eruptions accessed an atmospheric environment with high-energy ultraviolet radiation. Ash particles in the plume may have a very important role in preventing shorter wave UV radiation from photolyzing the SO_2 gas, but did not prevent stratospheric high-$\Delta^{17}O$, ozone-derived compounds from transferring their signature via net addition of ^{17}O-enriched oxygen to the SO_2 gas. The mass-independent signature of sulfur in Antarctic ice sulfate reported by Savarino et al. (2003b) may reflect special conditions over Antarctica where "old" stagnant air masses with seasonal lifespan of several months accumulate volcanogenic SO_2 and are exposed for a long time to shortest wave UV-radiation in the upper stratosphere due to deficiency of ozone layer shielding (e.g., Finlayson-Pitts and Pitts, 2000).

4.5. Mass-dependent sulfur isotope fractionation and interpretation of exponents and large $\delta^{34}S$ ranges

An important result of the present study is the observation of a possible difference in the mass-dependent fractionation exponents for large and small eruptions, with the range exceeding any other published dataset including those

involving microbial processes (cf. Johnston et al., 2005). The following discussion focuses on a subset of the Lava Creek tuff samples that form an array with $\delta^{33}S \sim 0.509$ $\delta^{34}S$ and $\delta^{36}S \sim 1.95$ $\delta^{34}S$ and have the largest range in "conventional" isotope ratios (Table 3 and Fig. 9). Although this is not the same as the equilibrium arrays $\delta^{33}S \sim 0.515$ $\delta^{34}S$ and $\delta^{36}S \sim 1.90$ $\delta^{34}S$ that are observed for small eruptions, we interpret this array to reflect mass-dependent processes in the framework of SO_2 oxidation. Below, we consider two possibilities used to describe the $\delta^{34}S$ systematics as discussed above: a mechanism dominated by kinetic isotope fractionation in a gas phase as suggested by Leung (2003); and Rayleigh distillation of SO_2 gas upon oxidation to the sulfuric acid. These simple calculations raise the intriguing prospect of mass-dependent constraints on sulfur chemistry in volcanic plumes. It is also clear that detailed computer modeling of sulfur transformation pathways is required before the constraints can be made quantitative.

4.5.1. Kinetic isotope fractionation

The most straightforward explanation for the exponents is that they reflect kinetic isotopic fractionation during the gas-phase reaction of SO_2 with OH (Table 3). Sulfur dioxide oxidation in the stratosphere may be primarily controlled this reaction (e.g., Fulle et al., 1999; Leung et al., 2001). However, if this mechanism plays a leading role in setting the isotopic systematics that we observe, then the preservation of primary kinetic fractionation exponents requires that mass balance was not an isotopically limiting influence. That is, an essentially infinite reservoir of SO_2 is implied. The attractive aspect of this possibility is that it suggests that the large amounts of SO_2 released after larger eruptions were processed via gas phase oxidation, as compared to the SO_2 from smaller volume eruptions, which may have underwent oxidation on aerosol surfaces. This should be verified by tracking rare isotope sulfur species through kinetic models of atmospheric SO_2 chemistry.

4.5.2. Rayleigh distillation

For the following analysis we begin by describing how Rayleigh distillation can change the exponentials that relate fractionations involving ^{32}S, ^{33}S, ^{34}S, and ^{36}S. The equations that describe Rayleigh distillation for the three isotope ratios of interest are:

$$^{3x}R/^{3x}R_0 = f^{(3x\alpha-1)} \quad (1)$$

where x stands for ^{33}S, ^{34}S, ^{36}S, and f is the fraction of total S remaining through its major isotope ^{32}S. Then, by dividing the equation of one sulfur isotope by that for another isotope and taking natural logarithms of both sides of the equations we obtain the following relationships (e.g., Blunier et al., 2002; Angert et al., 2003), and Assonov and Brenninkmeijer, 2005):

$$\frac{\ln(^{33}R/^{33}R_0)}{\ln(^{34}R/^{34}R_0)} = \frac{(^{33}\alpha - 1)}{(^{34}\alpha - 1)}, \text{ and} \quad (2)$$

$$\frac{\ln(^{36}R/^{36}R_0)}{\ln(^{34}R/^{34}R_0)} = \frac{(^{36}\alpha - 1)}{(^{34}\alpha - 1)}. \quad (3)$$

The fractionation factors given by $^{33}\alpha$, $^{34}\alpha$, and $^{36}\alpha$ are the intrinsic (i.e., actual/primary) fractionation factors involved in the Rayleigh process.

Fig. 10 presents the isotopic fractionation exponents associated with the residual reactants of a Rayleigh process as a function of the exponents for the underlying fractionation process, contoured for different $^{34}\alpha$ values. If an equilibrium process were responsible for the observed variation in the LCT samples, a large $^{34}S/^{32}S$ fractionation between SO_2 and product sulfate ($\sim$40–60‰) would be required (indicated by the intersection of the horizontal line and the narrow vertical bar on Fig. 10). Notice that the magnitude of the fractionation factor needed for this process to operate slightly overlaps with the range of $^{34}\alpha$ values predicted using vibrational frequency data and temperatures >0 °C. Our calculated values for SO_2–sulfate equilibrium sulfur isotope exchange at 0 °C yield $^{34}\alpha = 44‰$ and exponents of 0.514 and 1.90 to relate this to $^{33}\alpha$ and $^{36}\alpha$ (calculated using the methods of Urey, Herzberg, and Richet, referenced in Farquhar and Wing (2003).

Alternatively, if the $^{34}\alpha$ values of the fractionating SO_2 removal pathway are known, then Fig. 10 can be used to constrain the intrinsic fractionation exponents that would be required. If the $^{34}S/^{32}S$ fractionation between SO_2 and product sulfate is as large as predicted by Leung et al. (2001) ($\sim$100–160‰; gray band in Fig. 10) the LCT data

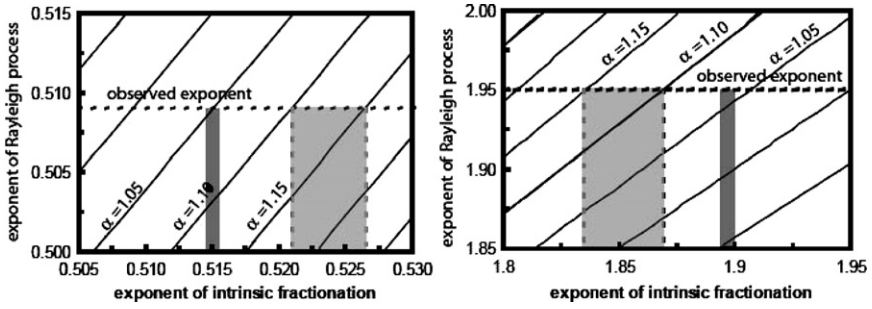

Fig. 10. Exponents of Rayleigh sulfur isotope fractionation vs. exponents of intrinsic fractionation of $^{33}S/^{32}S$ vs. $^{34}S/^{32}S$ and $^{36}S/^{34}S$ vs. $^{34}S/^{32}S$ isotope variations for different values of $^{34}\alpha(34\langle(SO_2–SO_4)$. The observed exponents for large caldera forming eruptions (Table 3) are shown by dashed lines; dark thin vertical bars indicates the equilibrium exponents, which would require 50–60‰ ($^{34}\alpha = 1.05–1.06$) fractionation to explain the Rayleigh slopes. Wide vertical rectangle indicate 110‰ to 150‰ ($^{34}\alpha = 1.10–1.15$) fractionation from Leung et al. (2001), which should yield the ranges of intrinsic exponents of 0.521–0.526 and 1.83–1.87, respectively, to be verified in future experiments using rare sulfur isotopes.

require intrinsic exponents of 0.521–0.527 (1.83–1.87) to relate $^{33}\alpha$ ($^{36}\alpha$) to the $^{34}\alpha$ for $SO_2 + OH$. These exponents are different from the values (<0.515 and >1.90, respectively) that would be determined using simplified representations of kinetic isotope fractionation (Fig. 9 and Table 3).

However, the counterintuitive result implied by our Rayleigh modeling using rare sulfur isotopes (Fig. 9 and 10) is that large mass-dependent range of sulfur isotope and exponents of $\delta^{33}S \sim 0.509$ $\delta^{34}S$ and $\delta^{36}S \sim 1.95$ $\delta^{34}S$ can only be explained by a *residual* Rayleigh reactant—SO_2 gas—rather than a Rayleigh product. Modeling of the Rayleigh *product*—precipitated sulfate—generally yields a non-zero intercept on a plot like Fig. 7. If this simple modeling captures the essence of the processes occurring in natural plumes, then the sampled sulfate represents oxidation of remaining residual SO_2 left on ash particles after the progressive loss of sulfate from the gas cloud. This implies at least two removal pathways for SO_2 in volcanic plumes: one removal pathway left behind residual SO_2 with substantial Rayleigh isotopic fractionations similar to those predicted by equilibrium considerations, while the other was isotopically insignificant, but led to formation of the pooled product sulfate precipitated from the cloud.

This interpretation may explain the difference between sulfur isotope systematics for caldera-forming eruptions and for smaller eruptions. If the ash sulfate actually represents the adsorption of residual SO_2 onto particles in the volcanic plume, it may be that larger eruptions provide enough reactive surfaces or sulfur dioxide to preserve an isotopic record in the deposited ash.

5. SUMMARY AND CONCLUSIONS

Our survey of Pleistocene ash beds in western US yielded moderate to strong $\Delta^{17}O$ signatures which, in conjunction with the results of Bao et al. (2003) on a large Oligocene ash unit, suggests that large caldera-forming eruptions are characterized by these isotopic features. We interpret these signatures to reflect stratospheric processing of SO_2 from the volcanic plume.

We observe a general negative correlation for $\Delta^{33}S$ vs. $\delta^{34}S$, and a positive correlation of $\Delta^{36}S$ vs. $\delta^{34}S$, for large caldera-forming eruptions and no correlation for small eruptions. The correlations likely reflect the sulfate formation and removal processes that occur in large caldera-forming eruptions. If these large eruptions reached the stratosphere and if most stratospheric sulfate forms (at least initially) through the gas-phase oxidation of SO_2 by OH (Fulle et al., 1999), our results may offer an observational constraint on ^{17}O, ^{33}S, and ^{36}S fractionation during this process.

Injection of large quantities of SO_2 gas may lead to the exhaustion of water (as well as OH and H_2O_2) in the volcanic plume environment; the SO_2 oxidation chemistry at high SO_2 loadings may lead to the "drying out" of the stratosphere (e.g., Bekki, 1995; Savarino et al., 2003b). Alternatively, if excess water is supplied with volcanic plume, stratospheric hydration is the possibility. When combined with $\Delta^{17}O$ measurements, our prediction regarding rare sulfur isotopic fractionation during OH-driven oxidation offers a tool to evaluate the stratospheric hydration/dehydration hypothesis. The mass-independent oxygen isotopic signature of ash–sulfate from caldera-forming eruptions implicates the involvement of stratospheric ozone in its formation. This result points to the need for quantitative investigations of significant ozone layer depletion as an additional volcanic hazard, which, in addition to the climatic impacts of sulfate aerosols, may affect the atmospheric environment for several years after major eruptions.

ACKNOWLEDGMENTS

We thank John Fournelle, John Pallister, and Olgeir Sigmarsson for sample donation, Kelli McCormick for help during S. Dakota field sampling, Art Bettis for Iowa and Nebraska sampling assistance, and Lena Bogolyubova for help with California sampling. John Valley for long-term collaboration on Yellowstone, Simon Poulson for analyses of barite for sulfur isotopes, Pat Shanks for providing barite standards, Axel Schmitt for trying barite analyses by SIMS, Nathan Dalleska for ICP-MS analyses of leachate solutions, and Paul Engelking for analysis of solutions using an ion chromatograph. Alex Pavlov and Jim Lyons are thanked for discussions on the atmospheric chemistry of sulfur and oxygen. University of Oregon (EAR-0537872 IB), Caltech (EAR-0345905 JE) are thanked for support of fieldwork and oxygen isotope analyses. Work at the University of Maryland was funded by EAR-0348382, NAG51235, and a fellowship of the Hanse Wissenschaftskolleg (J.F.), as well as NNG05GF86G and NNG05GQ 96G (J.F., B.A.W.). Reviews of two anonymous reviewers and Alex Pavlov, and editorial handling by Tom Chacko are acknowledged.

APPENDIX A. SUPPLEMENTARY DATA

Supplementary data associated with this article can be found, in the online version, at doi:10.1016/j.gca.2007.01.026.

REFERENCES

Alexander B., Thiemens M. H., Farquhar J., Kaufman A. J., Savarino J., and Delmas R. J. (2003) East Antarctic ice core sulfate sulfur isotope measurements over a complete glacial–interglacial cycle. *J. Geophys. Res.* **108**. doi:10.1029/2003JD00351. Article 4786.

Ambrose S. H. (1998) Late Pleistocene human population bottlenecks, volcanic winter, and differentiation of modern humans. *J. Hum. Evol.* **34**, 623–651.

Angert A., Rachmilevitch S., Barkan E., and Luz B. (2003) Effects of photorespiration, the cytochrome pathway, and the alternative pathway on the triple isotopic composition of atmospheric O-2. *Glogab Biogeochem. Cycles* **17**(1). Art. No. 1030.

Assonov S. S., and Brenninkmeijer C. A. M. (2005) Reporting small $\Delta^{17}O$ values: existing definitions and concepts. *Rapid Commun. Mass Spectrom.* **19**, 627–636.

Bao H. M. (2006) Purifying synthetic barite for oxygen isotope measurement by dissolution and reprecipitation in a chelating solution. *Anal. Chem.* **78**, 304–309.

Bao H. M. (2005) Sulfate in modern playa settings and in ash beds in hyperarid deserts: implication for the origin of ^{17}O-anomalous sulfate in an Oligocene ash bed. *Chem. Geol.* **214**, 127–134.

Bao H. M., Michalski G. M., and Thiemens M. H. (2001) Sulfate oxygen-17 anomalies in desert varnishes. *Geochim. Cosmochim. Acta* **13**, 2029–2036.

Bao H., Thiemens M. H., David B., Loope D. B., and Xun-Lai Yuan X.-L. (2003) Sulfate oxygen-17 anomaly in an Oligocene ash bed in mid-North America: was it the dry fogs? *Geophys. Res. Lett.* **30**, 1843–1848.

Bao H., and Thiemens M. H. (2000) Generation of O_2 from $BaSO_4$ using a CO_2-laser fluorination system for simultaneous analysis of $\delta^{18}O$ and $\delta^{17}O$. *Anal. Chem.* **72**, 4029–4032.

Baroni M., Thiemens M. H., Delmas R. J., and Savarino J. (2007) Mass-independent sulfur isotopic compositions in stratospheric volcanic eruptions. *Science* **315**, 84–87.

Bechtel C., and Zahn A. (2003) The isotope composition of water vapour: a powerful tool to study transport and chemistry of middle atmospheric water vapor. *Atmos. Chem. Phys. Discuss.* **3**, 3991–4036.

Bekki S., Pyle J. A., Zhong W., Toumi R., Haigh J. D., and Pyle D. (1996) The role of microphysical and chemical processes in prolonging the climate forcing of the Toba eruption. *Geophys. Res. Lett.* **23**(19), 2669–2672.

Bekki S. (1995) Oxidation of volcanic SO_2: a sink for stratospheric OH and H_2O. *Geophys. Res. Lett.* **22**, 913–916.

Bettis, E. A. III, Mason, J. P., Swinehart, J. B., Miao, X., Hanson, P. R., Goble, R. J., Loope, D. P., Jacobs, P. M., and Roberts, H.M. (2003) Cenozoic eolian sedimentary systems of the USA midcontinent. In *Quaternary Geology of the United States, INQUA 2003 Field Guide Volume* (ed. D. J. Easterbrook). Desert Research Institute, Reno, NV, pp. 195–218.

Bettis, E. A. III (ed). (1990) *Holocene Alluvial Stratigraphy and Selected Aspects of the Quaternary History of Western Iowa, Guidebook for the 37th field conference of the Midwest Friends of the Pleistocene*, Iowa City, 197 p. (reprinted as IDNR-Geological Survey Bureau Guidebook Series No. 9, Iowa City).

Bindeman I. N. (2006) Secrets of Supervolcanoes. *Scientific American* **294**, 26–33.

Blunier T., Barnett B., Bender M. L., and Hendricks M. B. (2002) Biological oxygen productivity during the last 60,000 years from triple oxygen isotope measurements. *Global Biogeochem. Cycles* **16**. doi:10.1029/2001GB00146.

Brasseur G., and Granier C. (1992) Mount Pinatubo aerosols, chlorofluorocarbons, and ozone depletion. *Science* **257**, 1239–1242.

Castleman J. A. W., Munkelwitz H. R., and Manowitz B. (1973) Contribution of volcanic sulphur compounds to the stratospheric aerosol layer. *Nature* **244**, 345–346.

Coffey M. T. (1996) The impact of volcanic activity on stratospheric chemistry. *J. Geophys. Res.* **101**, 6767–6780.

Farquhar J., Bao H., and Thiemens M. H. (2000) Atmospheric influence of Earth's earliest sulfur cycle. *Science* **289**, 756–758.

Farquhar J., Savarino J., Airieau S., and Thiemens M. H. (2001) Observation of wavelength-sensitive mass-independent sulfur isotope effects during SO_2 photolysis: implications for the early atmosphere. *J. Geophys. Res.* **106**, 32829–32839.

Farquhar J., and Wing B. A. (2003) Multiple sulfur isotopes and the evolution of the atmosphere. *Earth Planet. Sci. Lett.* **213**, 1–13.

Farquhar J., Johnston D. T., Wing B. A., Habicht K. S., Canfield D. E., Airieau S., and Thiemens M. H. (2003) Multiple sulphur isotopic interpretations of biosynthetic pathways: implications for biological signatures in the sulphur isotope record. *Geobiology* **1**, 27–36.

Finlayson-Pitts B.J., and Pitts J.N. (eds.) (2000) *Chemistry of the Upper and Lower Atmosphere: Theory, Experiments, and Applications*. Academic Press, San Diego, 969 pp.

Forrest J., and Newman L. (1977) Silver-110 microgram sulfate analysis for the short time resolution of ambient levels of sulfur aerosol. *Anal. Chem.* **49**, 1579–1584.

Fournelle J., Carmody R., and Daag A. (1996) Anhydrite-bearing Pumices from the June 15, 1991 Eruption of Mount Pinatubo: Geochemistry, Mineralogy, and Petrology. In: *Fire and Mud: Eruptions and Lahars from Mount Pinatubo, Philippines* (eds. C. G. Newhall and R. S. Punongbayan). PHIVOLCS-University of Washington, pp. 845–863.

Fulle D., Hamann H. F., and Hippler H. (1999) The pressure and temperature dependence of the recombination reaction $HO + SO_2 + M \Rightarrow HOSO_2 + M$. *Phys. Chem. Chem. Phys.* **1**, 2695–2702.

Eiler J. M., and Schauble E. (2004) $^{13}C^{18}O^{16}O$ in Earth's atmosphere. *Geochim. Cosmochim. Acta* **68**, 4767–4777.

Gerlach T. M., and McGee K. A. (1994) Total sulfur dioxide emissions and pre-eruption vapor-saturated magma at Mount St. Helens, 1980–88. *Geophys. Res. Lett.* **21**, 2833–2836.

Gonfiantini, R., Stichler, W., and Rozanski, K. (1995) In *Reference and Intercomparison Materials for Stable Isotopes of Light Elements*, IAEA-TECDOC-825, IAEA, Vienna, pp. 13–29.

Hulston J. R., and Thode H. G. (1965) Variations in ^{33}S, ^{34}S and ^{36}S contents of meteorites and their relation to chemical and nuclear effects. *J. Geophys. Res.* **70**, 3475–3484.

Izett G. A. (1981) Volcanic ash beds—recorders of upper Cenozoic silicic pyroclastic volcanism in the Western United States. *J. Geophys. Res.* **86**, 200–222.

Johnston D. T., Farquhar J., Wing B. A., Kaufman A. J., Canfield D. , and Habicht K. S. (2005) Multiple sulfur isotope fractionations in biological systems: a case study with sulfate reducers and sulfur disproportionators. *Am. J. Sci.* **305**, 645–660.

Khademi H., Mermut A. R., and Krouse H. R. (1997) Sulfur isotope geochemistry of gypsiferous aridisols from central Iran. *Geoderma* **80**, 195–209.

Krankowsky D., Lammerzahl P., and Mauersberger K. (2000) Isotopic measurements of stratospheric ozone. *Geophys. Res. Lett.* **27**, 2593–2595.

Larsen D., Swihart G. H., and Xiao Y. K. (2001) Hydrochemistry and isotope composition of springs in the Tecopa basin, southeastern California, USA. *Chem. Geol.* **179**, 17–35.

Lee C. C. W., Savarino J., and Thiemens M. H. (2001) Mass independent oxygen isotopic composition of atmospheric sulfate: Origin and implications for the present and past atmospheres of Earth and Mars. *Geophys. Res. Lett.* **28**, 1783–1787.

Leung, F.-Y. T. (2003) Elucidation of the Origins of Stratospheric Sulfate Aerosols by Isotopic Methods. PhD thesis. http://resolver.caltech.edu/CaltechETD:etd-05292003-144531.

Leung F. Y., Colussi A. J., and Hoffmann M. R. (2001) Sulfur isotopic fractionation in the gas-phase oxidation of sulfur dioxide initiated by hydroxyl radicals. *J. Phys. Chem. A* **105**, 8073–8078.

Lipman, P. W. (1975) Evolution of the Platoro Caldera Complex and Related Volcanic Rocks, Southeastern San Juan Mountains, Colorado, *US Geological Survey, Professional Paper* **852**, 128.

Loope D. B., Mason J. A., Bao H. M., Kettler R. M., and Zanner C. W. (2005) Deformation structures and an alteration zone linked to deposition of volcanogenic sulphate in an ancient playa (Oligocene of Nebraska, USA). *Sedimentology* **52**, 123–139.

Lyons J. R. (2001) Mass-independent fractionation of oxygen-containing radicals in the atmosphere. *Geophys. Res. Lett.* **28**, 3231–3234.

McKibben M. A., Eldridge C. S., Reyes A. G. (1996) Sulfur isotopic systematics of the June 1991 Mount Pinatubo eruptions: a SHRIMP ion microprobe study. In *Fire and Mud: Eruptions and Lahars from Mount Pinatubo, Philippines* (eds. Newhall and Punongbayan). PHIVOLCS-University of Washington, pp. 824–844.

McKinney C. R., McCrea J. M., Epstein S., Allen H. A., and Urey H. C. (1950) Improvements in mass spectrometers for the

measurement of small differences in isotope abundance ratios. *Rev. Sci. Instr.* **21**, 724–730.

Michalski, G., Rech, J., and Thiemens, M. (2005) The onset of hyper-aridity in the Atacama Desert: nitrate $\Delta^{17}O$ as a tracer of soil moisture. Goldschmidt conference abstracts A444.

Miller M. F. (2002) Isotopic fractionation and the quantification of ^{17}O anomalies in the oxygen triple-isotope system: an appraisal of geochemical significance. *Geochim. Cosmochim. Acta* **66**, 1881–1889.

Nelson S. T., Karlsson H. R., Paces J. B., Tingey D. G., Ward S., and Peters M. T. (2001) Paleohydrologic record of spring deposits in and around Pleistocene pluvial Lake Tecopa, southeastern California. *Geol. Soc. Am. Bull.* **113**, 659–670.

Ohmoto H., Watanabe Y., Ikemi H., Poulson S. R., and Taylor B. (2006) Sulphur isotope evidence for an oxic Archaean atmosphere. *Nature* **442**(7105), 908–911.

Ohmoto H., and Rye R. O. (1979) Isotope of sulfur and carbon. In *Geochemistry of Hydrothermal deposits* (ed. H. L. Barnes). John Wiley & Sons, pp. 509–567.

Ono S., Wing B. A., Johnston D. T., Farquhar J., and Rumble D. (2006) Mass-dependent fractionation of quadruple stable sulfur isotope system as a new tracer of sulfur biogeochemical cycles. *Geochim. Cosmochim. Acta* **70**, 2238–2252.

Oppenheimer C. (2002) Limited global change due to the largest known Quaternary eruption, Toba approximate to 74 kyr BP? *Quat. Sci. Rev.* **21**(14–15), 1593–1609.

Pavlov A. A., Mills M. J., and Toon O. B. (2005) Mystery of the volcanic mass-independent sulfur isotope fractionation signature in the Antarctic ice-core. *Geophys. Res. Lett.* **32**. Art. No. L12816.

Pierazzo E., Hahmann A. N., and Sloan L. C. (2003) Chicxulub and climate: radiative perturbations of impact-produced S-bearing gases. *Astrobiology* **3**, 99–118.

Pyle D. M., Beattie P. D., and Bluth G. J. S. (1996) Sulphur emissions to the stratosphere from explosive volcanic eruptions. *Bull. Volcanol.* **57**, 663–671.

Rampino M. R., and Self S. (1992) Volcanic winter and accelerated glaciation following the Toba super-eruption. *Nature* **359**, 50–52.

Robock A. (2002) Pinatubo eruption—the climatic aftermath. *Science* **295**, 1242–1244.

Robock A. (2000) Volcanic eruptions and climate. *Rev. Geophys.* **38**(2), 191–219.

Romero A. B., and Thiemens M. H. (2003) Mass-independent sulfur isotopic compositions in present-day sulfate aerosols. *J. Geophys. Res.* **108**, 4524.

Rose, Jr., W. I. (1977) Scavenging of volcanic aerosol by ash: atmospheric and volcanologic implications. *Geology* **5**, 621–624.

Sakai H. (1968) Isotopic properties of sulphur compounds in hydrothermal processes. *Geochem. J.* **2**, 29–49.

Sarna-Wojcicki A. M., Morrison S. D., Meyer C. E., and Hillhouse J. W. (1987) Correlation of upper Cenozoic tephra layers between sediments of the western United States and eastern Pacific Ocean and comparison with biostratigraphic and magnetostratigraphic age data. *Geol. Soc. Am. Bull.* **98**, 207–223.

Sarna-Wojcicki A. M., Shipley S., Waitt, Jr., R. B., Dzurisin D., and Wood S. H. (1981) Areal distribution, thickness, mass, volume, and grain size of air-fall ash from the six major eruptions of 1980. In *The 1980 Eruptions of Mount St. Helens*, vol. 1250 (eds. P. W. Lipman and D. R. Mullineaux). U.S. Geological Survey Professional Paper, Washington. p. 844.

Savarino J., Bekki S., Cole-Dai J. H., and Thiemens M. H. (2003a) Evidence from sulfate mass independent oxygen isotopic compositions of dramatic changes in atmospheric oxidation following massive volcanic eruptions. *J. Geophys. Res.—Atmosphere* **108**(D21). Art. No. 4671.

Savarino J. A., Romero J., Cole-Dai S., Bekki S., and Thiemens M. (2003b) UV induced mass-independent sulfur isotope fractionation in stratospheric sulfate. *Geophys. Res. Lett.* **30**. Art. No. 2131.

Solomon S. (1999) Stratospheric ozone depletion: a review of concepts and history. *Rev. Geophys.* **37**(3), 275–316.

Tanaka N., Rye D. M., Xiao Y., and Lasaga A. C. (1994) Use of stable sulfur isotope systematics for evaluating oxidation reaction pathways and in-cloud-scavenging of sulfur dioxide in the atmosphere. *Geophys. Res. Lett.* **21**, 1519–1522.

Taylor B. (1986) Magmatic volatiles: isotopic variations of C, H, and S. In *Stable Isotopes in high-temperature geologic processes, Rev. in Mineralogy*, vol. 16 (eds. J. W. Valley, H. P. Taylor, and J.R. O'Neil). Mineral Soc. Am., pp. 185–226.

Textor C., Graf H. F., Herzog M., and Oberhuber J. M. (2003) Injection of gases into the stratosphere by explosive volcanic eruptions. *J. Geophys. Res. Atm.* **108**(D19). Art. No. 4606.

Thiemens M. H. (2002) Mass-independent isotope effects and their use in understanding natural processes. *Israel J. Chem.* **42**, 43–54.

Thode H. G., Monster J., and Dunford H. B. (1961) Sulphur isotope geochemistry. *Geochim. Cosmochim. Acta* **25**, 159–174.

Thordarson T., Self, S. (2003) Atmospheric and environmental effects of the 1783–1784 Laki eruption: a review and reassessment. *J. Geophys. Res. Atm.* (D1). Art. No. 4011.

Vanstempvoort D. R., and Krouse H. R. (1994) Controls of delta-O-18 in sulfate—review of experimental-data and application to specific environments. *Environ. Geochem. Sulfide Oxidation ACS Sym. Ser.* **550**, 446–480.

Wallace P. J. (2003) From mantle to atmosphere: magma degassing, explosive eruptions, and volcanic volatile budgets. In *Melt inclusions in volcanic systems: methods, applications and problems* (eds. B. De Vivo and R. J. Bodnar). Elsevier, Amsterdam. pp. 105–127.

Webster C. R., and Heymsfield A. J. (2003) Water isotope ratios D/H, $^{18}O/^{16}O$, $^{17}O/^{16}O$ in and out of clouds map dehydration pathways. *Science* **302**, 1742–1745.

Young E. D., Galy A., and Nagahara H. (2002) Kinetic and equilibrium mass-dependent fractionation laws in nature and their geochemical and cosmochemical significance. *Geochim. Cosmochim. Acta* **66**, 1095–1104.

Zielinski G. A., Mayewski P. A., Meeker L. D., Whitlow S., Twickler M. S., and Taylor K. (1996) Potential atmospheric impact of the Toba mega-eruption similar to 71,000 years ago. *Geophys. Res. Lett.* **23**, 837–840.

Associate editor: Thomas Chacko